Constraints on Source and Attenuation Parameters
For moderate earthquakes in Central and Eastern North America

Final Report, NEHRP Grant G13AP00067 ***Gail M. Atkinson, November 2014***

ABSTRACT

This report describes the development of a method of estimating moment magnitude and stress drop for moderate events (**M** 3.5 to 6) in central and eastern North America (CENA) from regional ground-motion data. Ground-motion data include thousands of response spectra compiled for events of **M**3.5 to 6 as part of the NGA-East, NGA-West2 and seismotoolbox projects. The basic idea is to empirically characterize the relationship between observed spectral amplitudes at near-to-regional distances and seismic moment. The effective use of regional data to provide insight into source and attenuation is important, because near-source data are sparse in CENA. By considering both NGA-East and NGA-West2 databases, the study enables consistent comparisons of stress drops for events of the same moment amongst regions. The constraints that are provided by this study on source and attenuation parameters in CENA are important to the development of ground-motion prediction equations for use in the national seismic hazard maps, for accurate assessment and mitigation of earthquake hazards, and for ShakeMap applications in the East.

The report is divided into several sections, each of which stands alone. The first provides an introduction and overviews the general concepts used. The second presents the method to estimate moment **M**, while the third describes a comprehensive model of ground motions in CENA. Finally, the fourth section provides a recipe by which the study components can be easily used to obtain moment and stress drop for events from response spectral parameters commonly available through ShakeMap applications, and also provides source parameter estimates for the CENA events in the NGA-East database.

1 - Introduction

This project explores basic source parameters – moment magnitude and stress drop – for moderate events in Central and Eastern North America (CENA), and places constraints on ground-motion attenuation in CENA, particularly within 50 km and across the transition zone to Lg spreading (from 50 to 150 km). The model developed in the study accomplishes the following: (i) produces a catalogue of estimated moment magnitudes and stress drops for moderate events recorded on regional networks in CENA, in comparison to consistently-obtained source parameters for California events; (ii) provides insight into attenuation in CENA; and (iii) provides a fast and reliable model to estimate seismic moment and stress drop from ShakeMap parameters, for future events. A calibrated ground-motion prediction equation (GMPE) for CENA based on stochastic point-source modeling of the NGA-East database is also provided. These research products are very useful for GMPE development, seismic hazard estimation, and for ShakeMap applications.

The methodology is largely empirical in nature, with use of a simple stochastic point-source model (Boore, 2003) to provide a Brune-model context for basic source parameters (seismic moment and stress drop). The focus is on the moderate events (**M**<6) that make up the CENA database.

Background and Database

An understanding of basic ground-motion characteristics - in particular their near-source amplitudes and how they scale with magnitude and attenuate with distance - is crucial to accurate assessment and mitigation of earthquake hazards. In CENA the characterization of ground motion is subject to particularly large uncertainties, due to the paucity of data from strong earthquakes, and at short distances. The large uncertainties and relative lack of confidence in our assessment of the expected motions is a significant impediment to reducing urban seismic risk: without a confident and unambiguous assessment of hazard and ground motions, decision-makers are reluctant (with some justification) to spend limited resources on mitigation. It is thus crucial to reduce uncertainty in the characterization of CENA ground motions to enable progress on seismic hazard assessment and mitigation.

Knowledge of the attenuation of motions is especially needed at distances R<50km (due to their significance to hazard), but is also important through the "transition zone", where direct waves are joined by post-critical reflections from the Moho, and out to regional distances dominated by Lg-phase spreading. The attenuation needs to be understood over a broad range of distances so that we can "tie together" observations at distance with motions near the source. Attenuation studies in the East have focused on the data available in the northeastern U.S./southeastern Canada (e.g. Atkinson, 2004) due to the availability of recordings on rock sites in that region. Recent studies (Babaie Mahani and Atkinson, 2013; Hassani and Atkinson, 2014) suggest that the attenuation and source parameters are not significantly different in the central United States than in the more eastern regions of the continent. Hence we can analyze CENA as a single large region for the purposes of ground motion and attenuation studies.

Regional ground-motion investigations can be conducted using data from small-to-moderate events recorded on ANSS (Advanced National Seismic System) and affiliated broadband seismographic stations in CENA and elsewhere (where "ANSS" is often used loosely to include all ground-motion recording stations, including velocity and acceleration sensors from a number of cooperating networks). Many of these data have been compiled as part of the NGA-East (www.peer.berkeley/ngaeast/), NGA-West (www.peer.berkeley/ngawest/) and Seismotoolbox (www.seismotoolbox.ca) projects. Figures 1 to 2 provide maps of the events for which we have available ground-motion amplitudes for model development and comparisons from the NGA projects; recording station locations are also shown. The maps cover the study regions of the central U.S. (CUS, including New Madrid and surrounding regions), northeast U.S./ southeastern Canada (NEUS), northern

Califoria (NCal) and southern California (SCal). For the events shown on these maps, the NGA projects have already compiled the response spectra data (PSA, 5% damped pseudo-acceleration, horizontal and vertical components). There are also some additional data for the NEUS region in the seismotoolbox, which is regularly updated to include significant new events. The moment magnitude determinations performed by Prof. R. Herrmann (http://eqinfo.eas.slu.edu/Earthquake_Center/MECH.NA/MECHFIG/mech.html) for many of these events make them particularly valuable for calibration of attenuation and source studies, as will be discussed in more detail later. We include both the eastern and western data in the small-to-moderate magnitude range in this study, to enable consistent inter-regional comparisons of source and attenuation characteristics.

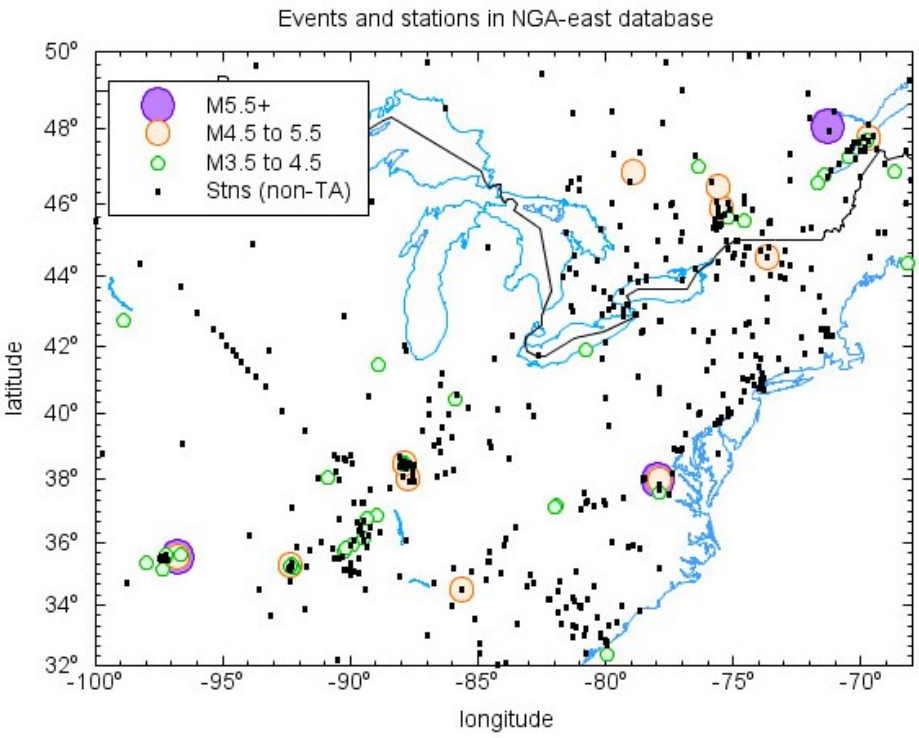

Figure 1 – Map of earthquakes and permanent stations in the CUS (lower left) and NEUS (upper right) for which we have compiled ground-motion data (from NGA-East). (Transportable-array stations not shown.)

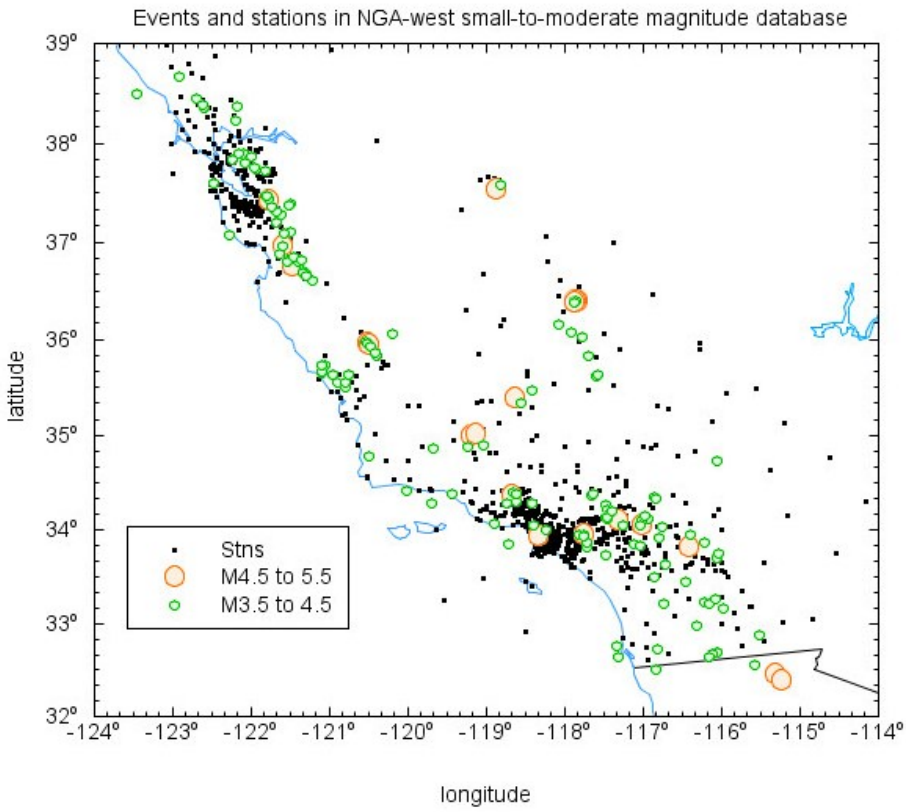

Figure 2 – Map of earthquakes and permanent stations in California for which we have compiled ground-motion data (from NGA-West; only the small-to-moderate magnitude dataset is shown here).

An understanding of attenuation is a pre-requisite to obtaining reliable estimates of source parameters for CENA earthquakes, as these source parameters must be estimated from observations gathered at distance. Source parameters, in turn, are critical to the prediction of ground-motion amplitudes at near-source distances and their scaling with magnitude, which is the focus of GMPEs for hazard applications. In particular, we require an understanding of the linked behavior of source and attenuation characteristics to make meaningful progress in predicting ground-motion amplitudes for future large earthquakes in the CENA. The linkage of source and attenuation parameters is an important "trade-off" problem in the development of GMPEs (e.g. Boore et al., 2010).

Seismic moment has an important role to play in constraining the source versus attenuation trade-off in ground-motion modeling. Consider Figure 3, which plots the Brune model Fourier acceleration spectrum (Brune, 1970; Boore, 2003) at a reference hypocentral distance of R_{hypo}=1 km, for earthquakes of **M**3.5 to 6.5, for stress drops ($\Delta\sigma$) of 50 and 500 bars (spanning the usual range for CENA events). The Brune spectral model is typically the basis for the source spectrum as prescribed by stochastic ground-motion simulations in the development of ground-motion prediction equations (GMPEs) for the CENA (eg. Toro et al., 1997; Frankel, 1996; Atkinson and Boore, 2006; Pezeshk et al., 2011). In this model, the long-period displacement level is proportional to moment, and thus the acceleration spectrum rises as frequency-squared, to the "corner frequency", above which it attains a constant value that depends on stress drop. The corner frequency depends on moment and stress drop; thus stress drop is a key unknown parameter in such models. The importance of stress drop for ground motions at high frequencies is apparent in Figure 3. For example, for **M**6.5 the high-frequency motions for a 500-bar event exceed those from a 50-bar event by a factor of about 5. The high-frequency decay parameter, kappa (Anderson and Hough, 1986), is also significant, especially at f>5Hz. At low frequencies, the Fourier spectrum at the source is entirely constrained by the moment magnitude (and a scaling constant). For small-to-

moderate events (**M**<5), the "moment end" of the spectrum effectively constrains near-source ground motions for frequencies up to ~1 Hz.

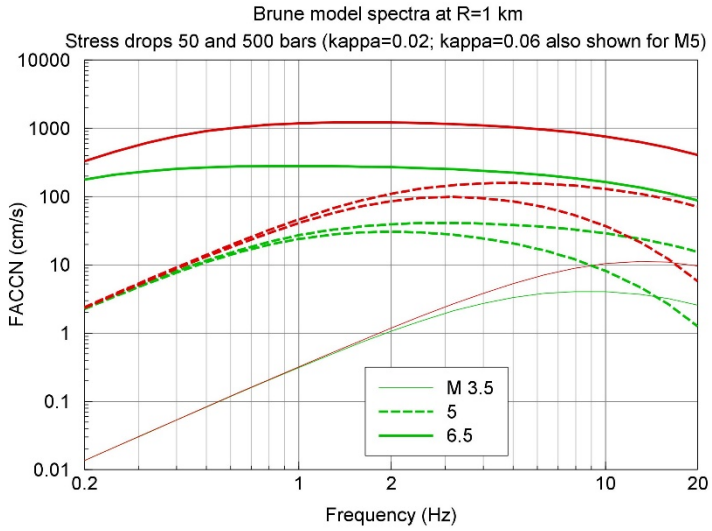

*Figure 3 – Fourier spectrum of acceleration (at R_{hypo}= 1 km) for Brune source model, for **M**=3.5, 5.0, 6.5, with stress drop parameters of 50 bars (green) and 500 bars (red), for kappa=0.02. Influence of kappa is illustrated by also plotting curves for kappa=0.06 at **M**5 (lower dashed curves for **M**5).*

Methodology

In this research program, several inter-related studies were conducted, in order to develop a methodology to determine basic source parameters (moment magnitude and Brune stress parameter) for events of **M**3.5 to 6.5 from regional ground-motion data. The underpinning of the methodology is an effective point-source stochastic model of ground motion, as described by Boore (2003, 2009) and Yenier and Atkinson (2014a). The methodology is general in nature and can be applied to both eastern and western events. This transportability of methodology is important because it enables consistent determination of eastern and western source and attenuation parameters for comparative purposes, which is very useful. For example, one of the preferred methods of GMPE development in the east, the hybrid-empirical method (Campbell, 2003; Pezeshk et al., 2011), relies on comparison of eastern vs. western stress drops.

The first component of the methodology is the determination of moment magnitude. In Section 2, I describe the use of 1-Hz response spectral amplitudes to estimate moment magnitude, using a calibrated point-source simulation model, for small-to-moderate events. (Note: moment magnitude for larger events, of **M**>4, is typically available from regional or global centroid moment tensor solutions, hence the focus of this study on reliable moments for smaller events.) This work has been published in Seismological Research Letters (Atkinson et al., 2014). Note that in this study, many simplifications are made in order to get an estimation formula that is efficient to use in practice. An alternative to use of Section 2 in estimation of moment magnitude would be to use the more detailed approach described in Section 3, which would be robust over a wider range of magnitudes and distances. Alternatively, one could use the calibration-based moment magnitude estimate derived for events at regional distances, as described in Atkinson and Babaie Mahani (2013). All three of these possible algorithms give similar values of moment for most events, and the choice between them is a matter of convenience and suitability for the application.

In Section 3, the simulation modeling approach is extended to derive a generic GMPE for eastern events, taking advantage of the NGA-East database. The model developed is tied to a corresponding model derived in analogous fashion from the more comprehensive NGA-West2 database. This novel study introduces a number of new concepts in stochastic point-source modeling, including an approach to decouple spectral shape from

amplitude level (through the use of a calibration constant) to provide more meaningful estimates of stress parameter, which are independent of the preferred model for geometric spreading. For the events in the NGA-East database, the stress parameter is determined based on the shape of the attenuation-corrected source spectrum. This work has been submitted for possible publication in the Bulletin of the Seismological Society of America (Yenier and Atkinson, 2014b).

Finally, in Section 4, I describe how we can use the simulation-based GMPE of Section 3 to rapidly determine both **M** (moment magnitude) and stress parameter for any moderate event that occurs in CENA, based on PSA at 1 Hz (to determine **M**), and PSA at 10 Hz or PGA (to determine stress parameter). This in turn allows the definition of a calibrated event-specific GMPE that can be used in ShakeMap applications.

References

Anderson, J. and S. Hough (1984). A model for the shape of the Fourier amplitude spectrum of acceleration at high frequencies. Bull. Seism. Soc. Am., **74**, 1969-1993.

Assatourians, K., and G. Atkinson (2010). Database of processed time series and response spectra for Canada: An example application to study of the 2005 MN5.4 Riviere du Loup, Quebec earthquake. Seism. Res. L., **81,** 1013-1031.

Atkinson, G. (2004). Empirical attenuation of ground motion spectral amplitudes in southeastern Canada and the northeastern United States. Bull. Seism. Soc. Am.,**94**, 1079-1095.

Atkinson, G. and A. Babaie Mahani (2013). Estimation of moment magnitude from ground motions at regional distances. Bull. Seism. Soc. Am., **103**, 107-116.

Atkinson, G. and D. Boore (2006). Ground motion prediction equations for earthquakes in eastern North America. Bull. Seism. Soc. Am., **96**, 2181-2205.

Atkinson, G., W. Greig and E. Yenier (2014). Estimation of moment magnitude for small events (M<4) on local networks. Seism. Res. L., **85**, 1116-1124.

Babaie Mahani, A. and G. Atkinson (2013). Regional differences in ground-motion amplitudes of small-to-moderate earthquakes across North America. Bull. Seism. Soc. Am., **103**, 2604-2620.

Boore, D. M. (2009). Comparing stochastic point-source and finite-source ground-motion simulations: SMSIM and EXSIM. Bull. Seismol. Soc. Am. **99**, 3202-3216.

Boore, D. (2003). Prediction of ground motion using the stochastic method. Pure and Applied Geophysics, **160**, 635-676.

Boore, D., K. Campbell and G. Atkinson (2010). Determination of stress parameters for eight well-recorded earthquakes in eastern North America. Bull. Seism. Soc. Am., **100**, 1632-1645.

Brune, J. (1970). Tectonic stress and the spectra of seismic shear waves from earthquakes. J. Geophys. Res., **75**, 4997-5009.

Frankel, A., C. Mueller, T. Barnhard, D. Perkins, E. Leyendecker, N. Dickman, S. Hanson and M. Hopper (1996). National seismic hazard maps, June 1996. U.S. Geol. Surv. Open-file Report 96-532.

Hassani, B. and G. Atkinson (2014). Referenced Empirical Ground Motion Prediction Equation for eastern North America. Seism. Res. L., in press.

Petersen, M., Frankel, A., Harmsen, S., Mueller, C., Haller, K., Wheeler, R., Wesson, R., Zeng, Y., Boyd, O., Perkins, D., Luco, N., Field, E., Wills, C., and Rukstales, K. (2008). Documentation for the 2008 Update of the United States National Seismic Hazard Maps: U.S. Geological Survey Open-File Report 2008–1128, 61 p.

Pezeshk, S., A. Zandieh and B. Tavakoli (2011). Ground-motion prediction equations for eastern North America from a hybrid empirical method. Bull. Seism. Soc. Am., **101**, 1859-1870.

Toro, G., N. Abrahamson and J. Schneider (1997). Model of strong ground motion in eastern and central North America: Best estimates and uncertainties. Seism. Res. L., **68**, 41-57.

Yenier, E. and G. Atkinson (2014a). Point-source modeling of moderate-to-large magnitude earthquakes and associated ground-motion saturation effects. Bull. Seism. Soc. Am., **104**, 1458-1478. DOI 10.1785/0120130147.

Yenier, E. and G. Atkinson (2014b). Regionally-Adjustable Generic Ground-Motion Prediction Equation based on Equivalent Point-Source Simulations: Application to Central and Eastern North America, Bull. Seism. Soc. Am., submitted.

2 - Estimation of moment magnitude (M) for small events (M<4) on local networks

(Gail M. Atkinson, D.Wesley Greig, and Emrah Yenier; as published in Seism. Res. L., 2014)

Section Summary

We develop a simple model to estimate moment magnitude for events of **M**<4, at distances out to ~300km, based on readily-available ShakeMap parameters and seismological scaling principles. Estimates of moment magnitude for such small events are not available from standard methods, but are needed for local-network applications and for traffic light systems for induced seismicity applications; this issue is currently of particular interest in central and eastern North America. The method takes advantage of the fact that for small events the response spectrum is well-correlated with seismic moment for periods greater than 0.3s, and can be predicted from a simple stochastic point-source model. We develop an equation by which we calculate M from the 1s PSA (**M**≥3) or the 0.3s PSA (**M**<3) at each station, using a simple linear equation that corrects for the effects of attenuation. We show that this method produces unbiased estimates of moment magnitudes in both eastern and western North America, for events of M≤4 recorded at distances <300 km.

Introduction

This section outlines a simple method to estimate moment magnitude (**M**) (Hanks and Kanomori, 1979) for small events (**M**<4) based on recorded ground motion parameters from a local seismographic network. The focus here is on small events, as the seismic moment (and hence **M**) from larger events can be obtained from standard seismological methods using regional and/or global data. For example, global and regional seismic moment tensor solutions are routinely available in most of North America for events of M>3.5 from the Univ. of St. Louis website of R. Herrmann (http://www.eas.slu.edu/eqc/eqcmt.html), or from the Global Moment Tensor catalogue for events of **M**>4.5 (www.globalcmt.org). The challenge to be addressed is reliable and robust estimation of size for small events (**M**<4), particularly the very small events (**M**≤3) that may only be recorded above noise at close distances. Reliable moment estimates are difficult to obtain for such events with either conventional moment estimation methods, or with methods based on calibration of regional data. Obtaining reliable moment estimates for small events is an important problem for two common seismological applications: (i) developing magnitude-recurrence relations for regions that merge small-event and large-event seismicity catalogues; and (ii) for induced-seismicity applications, in which traffic light protocols for responding to induced events require a reliable assessment of moment magnitude. These applications are currently of great interest in central and eastern North America (ENA).

The proposed method is based on vertical-component 5%-damped pseudo-acceleration amplitudes (PSA) at 1s or 0.3s. (Note: PSA at 1s is defined as the maximum displacement, in response to the ground motion, of a single-degree-of freedom 5%-damped oscillator, having a natural vibration period of 1s, multiplied by the factor $(2\pi)^2$). Response spectra at 1s and 0.3s are commonly-used parameters in engineering seismology; for example, both of these are standard ShakeMap parameters (Wald et al., 1999). Moreover, PSA at 1s and 0.3s provide a stable estimate of low-frequency ground motion for small events that is closely correlated with seismic moment. Recently, Atkinson and Babaie Mahani (2013) showed that reliable estimates of **M** may be obtained for moderate events in North America (**M** 3 to 5) using PSA at 1s recorded at regional distances (150 to 500 km), using a technique that employs calibration to moderate events with known moment magnitude. This technique

is useful for moderate events, but may not be useable for the small events (**M**<3) that are particularly important for induced seismicity applications, because such events may not have adequate signal-to-noise ratio at 1s at regional distances. Moreover, due to the lack of calibration events with known **M**, the method would rely on extrapolation of the calibration-based equations beyond the magnitude range in which they were defined, and might thus be significantly biased. Therefore, we need a modified approach that will make optimal use of local network data over a range of distances from short (<20 km) to regional (< 300 km), and that will have a reliable basis when applied to small events for which independent **M** estimates are not available for calibration. The purpose of this chapter is to describe such an approach. This provides an additional tool to that given by Atkinson and Babaie-Mahani (2013). Either tool can be used in estimating moments, depending on the application under consideration. Alternatively, the more detailed approach described in Section 3 can be used to estimate moment.

Method for Estimating M for small events

In this study, we develop a robust method of estimating **M** from PSA at 1s or 0.3s from local network data, focusing on short-to-regional distances, and using a stochastic point-source model to provide a physically-based scaling of the relationship down to small magnitudes. The vertical component PSA at 1s (PSA_1) is selected as the preferred parameter for our method – though as discussed further in the following, we also use PSA at 0.3s ($PSA_{0.3}$) for small events (**M**<3) to allow for greater signal-to-noise ratio. We use the vertical component because it minimizes the influence of site response, and is applicable to a range of sites which may have unknown site conditions. In general, vertical-component PSA will be similar to an unamplified horizontal-component PSA (see Lermo and Chavez Garcia, 1993; Siddiqqi and Atkinson, 2002; Atkinson and Boore, 2006).

For events of **M**<4, 1s is on the flat "low frequency" end of a standard Brune (1970) model displacement spectrum, where the amplitude is directly proportional to seismic moment, as shown on Figure 1. Moreover, for sufficiently small events, M<3, 0.3s is also on the low-frequency end of the spectrum, over a wide range of stress drop values. We use this basic seismological principle to formulate the method to estimate M. At 1s, PSA will scale with seismic moment in a manner that is practically independent of stress drop; the same is true for 0.3s PSA, if the event is of **M**<3. This simple point-source model is appropriate for the small events of interest here, and has been shown to be a reasonable model for ground motions in many parts of the world; see Boore (1983; 2003) for examples and a discussion of the seismological principles involved. The response spectrum is similar to a Fourier spectrum, though not identical as the response spectrum shows the maximum response of an oscillator to a record, while the Fourier spectrum is a more direct measure of its amplitude at each frequency. Atkinson (2012) shows the relationship between Fourier and response spectral amplitudes for small events in ENA.

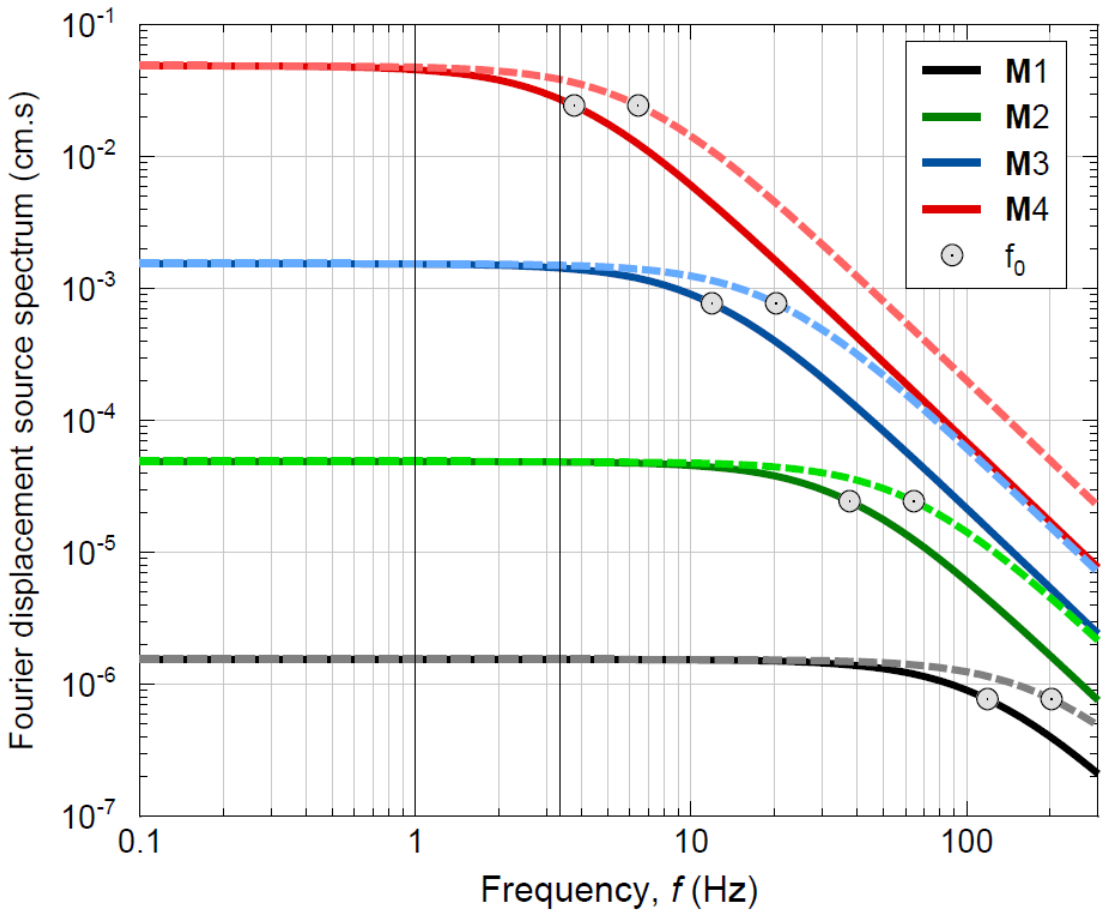

*Figure 1 – Source spectrum (at R=1km) for **M**=1, 2, 3, 4, for stress drop values of 100 bars (solid lines) and 500 bars (dashed lines) for Brune point-source model (neglecting high-frequency effects of kappa). Circles show corner frequencies and vertical black lines highlight 1Hz (=1s) and 3.3Hz (=0.3s).*

The approach taken is to use a model-driven ground-motion prediction equation (GMPE) for PSA_1 and $PSA_{0.3}$, formulated as a function of M and distance, as a tool from which to calculate M at each station. To do this, we use the stochastic point-source algorithm SMSIM (Boore, 2000) to simulate time series for events of M 0 to 4 (in increments of 0.2 units), at distances from 1 to 300 km (in increments of 0.1 log units), from which we calculate the average PSA at 1s and 0.3s. The model-based GMPE is an equation we define to express PSA_1 and $PSA_{0.3}$ as a simple function of M and the distance to the hypocenter (R). The underlying assumptions in these predictions, and their justification, are as follows:

1) the vertical component has minimal site amplification; thus no crustal or site amplifications are applied. This is consistent with a simplified interpretation of the relationship of horizontal-to-vertical spectral ratio to site response (Lermo and Chavez-Garcia, 1993; Siddiqqi and Atkinson, 2002), and has been applied in previous GMPEs, such as Atkinson and Boore (2006).

2) we assume a hinged bilinear form for the attenuation model, following Babaie Mahani and Atkinson (2013) and Yenier and Atkinson (2014); the geometrical spreading is modeled as $R^{-1.3}$ and $R^{-0.5}$ at distances ≤ 50 km and >50 km, respectively.

3) the stress drop is 300 bars for "western" regions, or 600 bars for "eastern" regions; these values are consistent with the adopted attenuation models, according to empirical data analyses in the two regions, as

shown by Atkinson and Boore (2014) for ENA and Yenier and Atkinson (2014) for western North America (WNA). (Note: In Chapter 3 we subsequently refine the stress parameters using a shape-based technique; however the results presented herein are not sensitive to stress drop, as we show, so this difference is unimportant.)

4) anelastic attenuation, is represented by a whole-path Q given as $Q = \max(170f^{0.45},100)$ for "western regions" (Raoof et al., 1999) or $Q = 525f^{0.45}$ for "eastern regions" (Atkinson and Boore, 2014) (where f is frequency).

5) duration is given by $1/f_0 + 0.05R$ in all regions, where f_0 is the corner frequency (which depends on moment and stress drop as described by Boore, 2003); the duration model is one that is commonly-adopted for point-source simulations (Boore, 2003; Atkinson and Silva, 2000; Atkinson et al., 2009).

6) near-surface attenuation is represented with the kappa parameter (Anderson and Hough, 1984), assuming $\kappa_0 = 0.02$s; this is a typical value for competent sites with minimal site effects (e.g. Atkinson and Boore, 2006; Campbell, 2009).

Figure 2 plots the simulated $PSA_{0.3}$ and PSA_1 amplitudes for both eastern and western attenuation models, along with the simplified function that we have defined as a basis for the magnitude estimation:

$$\log PSA_T = C_T + 1.45\mathbf{M} - \log Z(R) - \gamma_T R \qquad (1a)$$

where γ represents the coefficient of anelastic attenuation and $Z(R)$ is the geometrical attenuation that is given by

$$\log Z(R) = \begin{cases} 1.3\log R & R \leq 50\ km \\ 1.3\log 50 + 0.5\log(R/50) & R > 50\ km \end{cases} \qquad (1b)$$

The logarithmic terms are in base 10. R is hypocentral distance in km, and PSA is in cm/s^2. Note that Equation 1 employs the same geometrical attenuation model used for the simulations, which is a simplification/approximation, as shown in more detail in Chapter 3. Table 1 gives the values of the coefficients that correspond to the lines on Figure 2, and which define our adopted ground-motion model that is used in estimation of **M**.

Table 1 – Coefficients of adopted ground-motion model for M estimation (Equation 1)

	WNA		ENA	
	0.3s	1.0s	0.3s	1.0s
C_T	-3.15	-4.25	-3.3	-4.5
γ_T	0.005	0.0035	0.0015	0.0007

The equation is very simple, because the scaling of PSA at 0.3s and 1s is very regular for small events (Figure 1); we caution that this equation would generally underestimate **M** if applied to events of **M**>4, as it does not consider saturation effects that come into play when modeling larger events as a point source. The defined lines are not a regression fit to the simulated points, but rather represent the overall trends, in particular the magnitude-scaling indicated by the simulations from **M**0 to **M**4 at typical local-network distances of 5 to 50 km. The offset of the lines from the simulated values, apparent on Figure 2, reflects an empirical calibration factor that we use to ensure a good fit of the model equations to observations in both WNA and ENA, as

discussed in the next section. Essentially, we used the simulations to determine the magnitude scaling that we wished to impose on our ground-motion amplitude model. Then, with the geometric spreading and magnitude scaling held fixed, we calibrated the C_T and γ_T terms based on the empirical ground-motion data (next section) to determine their values, as given in Table 1. We note that if we had simply regressed the simulated amplitudes to obtain the coefficients of Equation 1, we would obtain very similar values to those in Table 1, but the constant C would be approximately 0.3 units lower in WNA, and 0.1 units lower in ENA, for the simulated values. This offset between simulations and observations reflects model misfits attributable to factors such as unmodeled source and site effects and the effect of noise on observed PSA, and is discussed in more detail in Section 3.

In Table 1, we have given variants for two typical regional γ values, which are applicable to active tectonic regions such as WNA and stable continental regions such as ENA. This primarily affects the term in R, though there is also a difference in the constant, due to the calibration to observed regional ground-motion amplitudes. The coefficient in R and the overall constant term can be adjusted where warranted on a regional basis using empirical observations, without affecting the overall magnitude scaling that is constrained by the Brune point-source model.

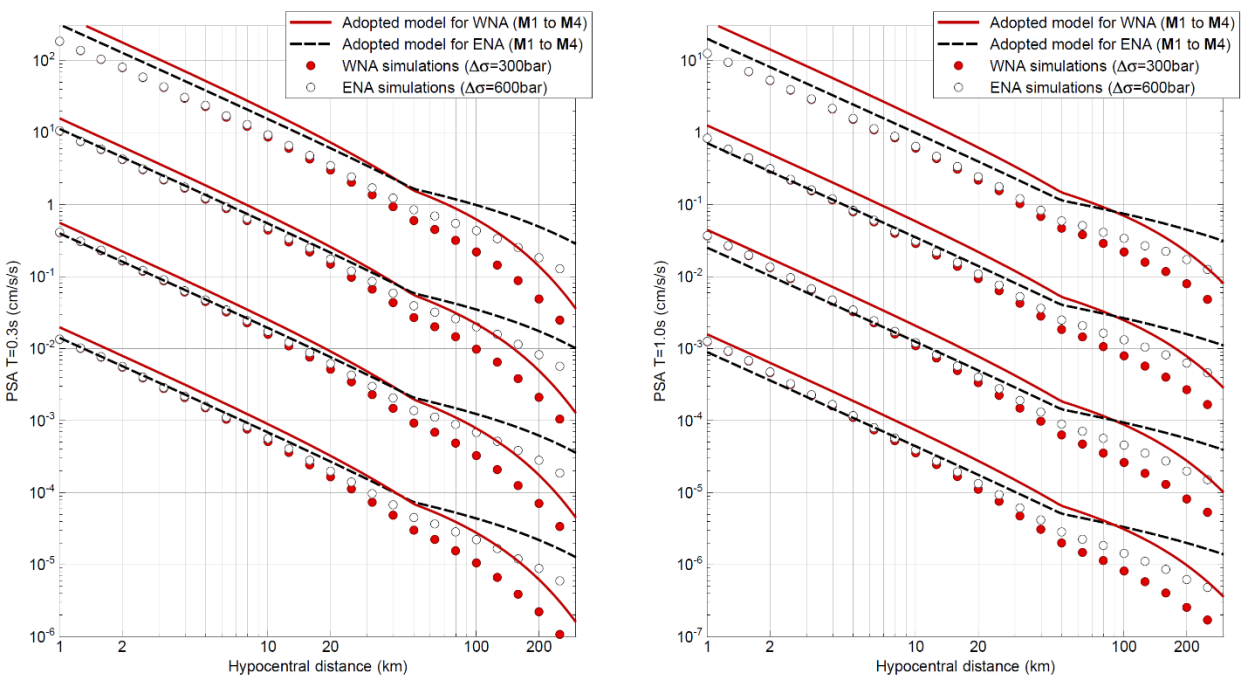

Figure 2 – Adopted model of vertical-component PSA at 0.3s (left) and 1s (right) as a function of hypocentral distance based on SMSIM point-source simulations. Points show simulation results, lines show model defined to represent simulation points, after calibration with empirical data (Equation 1).

We invert Eqn 1 to write an expression to calculate M at a station based on measured PSA_1 or $PSA_{0.3}$:

$$\mathbf{M} = (\log PSA_T - C_T + \log Z(R) + \gamma_T R)/1.45 \qquad (2)$$

with the coefficients as listed in Table 1. To apply this estimation method to recorded PSA data, we assume that $R=\sqrt{(D^2+h^2)}$, where D is epicentral distance and h is focal depth. For local network applications, we recommend assigning a nominal depth of 5 km to all events to ensure stability. The reason we fix the depth is that it may not be well determined initially; the actual depth value is not critical in this application, as long as it is reasonable (e.g. the magnitude will be relatively insensitive to depth within the range of focal depths from 1 to 20 km). The average M for an event is determined by averaging M estimates obtained over all stations for which we have a reasonable signal to noise ratio (e.g. a factor of three).

Calibration and Evaluation of Performance

We used ground-motion databases to calibrate the overall level of the **M** formulation equation and to test its performance. For WNA, we use the NGA-W2 ground-motion database (www.peer.berkeley.edu), which at small magnitudes is comprised of data from California. Figure 3 plots the data amplitudes of $PSA_{0.3}$ and PSA_1 in comparison to the prediction equations for WNA. It is important to note there are no data in the database for **M**<3, and thus the curves can only be compared to data for events of **M**≥3. A small initial mismatch in overall amplitude level between the simulations and the observations was corrected by an appropriate choice of the constant term in Equation 1, which is equivalent to applying a calibration factor; this is the source of the offset seen in Figure 2 between the defined prediction lines and the simulation amplitudes. It is interesting that the offset, and hence the calibration factor required, is greater in WNA than in ENA (0.3 log units versus 0.1 units). This may reflect greater site amplification effects that are present on the vertical component in WNA, due to the gradational shear-wave velocity profile. Overall, Figure 3 shows that there is good agreement between the observed PSA data and the defined model equations, in both amplitude level and attenuation shape, suggesting that the model is generally applicable and that the assumed attenuation is reasonable.

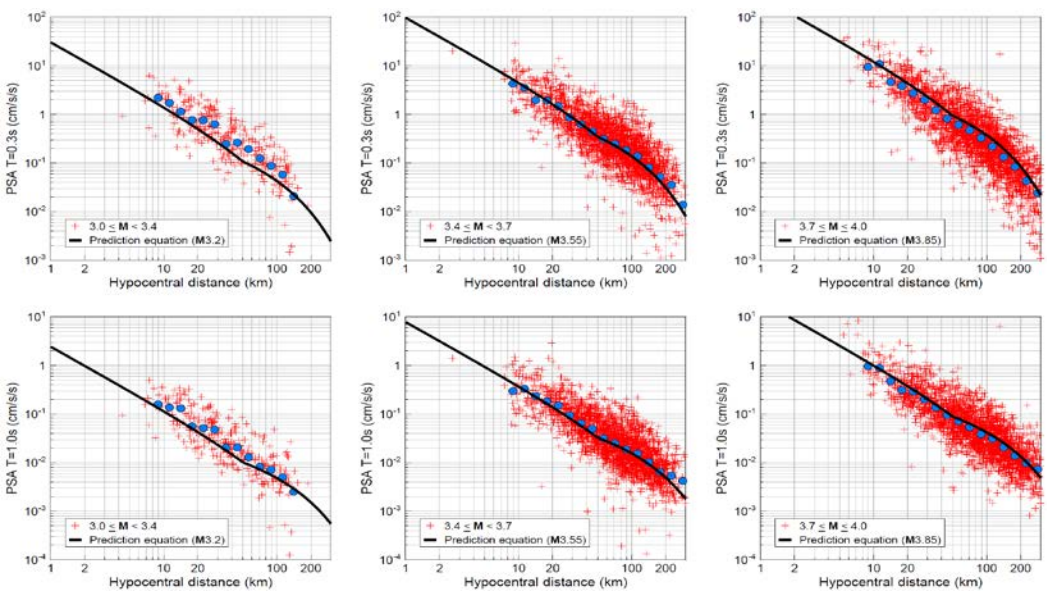

*Figure 3 – Comparison of Equation 1 (lines), evaluated at **M**=3.2, 3.55 and 3.85, with WNA ground-motion data (plus symbols), for PSA at 0.3s (top) and 1.0s (bottom). Circles show average data amplitudes in distance bins.*

Figure 4 provides a more quantitative evaluation of how well the proposed **M** estimation model (Eqn 2) works for the NGA-W2 database. For each observation with **M**≤4 and *R*≤300 km, we calculate **M** from Eqn 2 (with *C*=-4.25 and γ=0.0035) and compare it to the known value of M tabulated in the NGA-W2 database, to define the **M** bias (e.g.$M_{i,known} - M_{ij,predicted}$, where $M_{i,known}$ represents the known **M** of event *i* and $M_{ij,predicted}$ denotes the predicted **M** for the same event using the PSA obtained at station *j*). By plotting the bias versus distance in several magnitude ranges, we observe that the equation works well for events of **M** 3 to 4, at distances up to 300 km, with no significant trends. Moreover, comparing the known **M** with the estimated values, for earthquakes having three or more observations within 300 km, we note that predictions generally lie within ± 0.1 units of the known magnitude value.

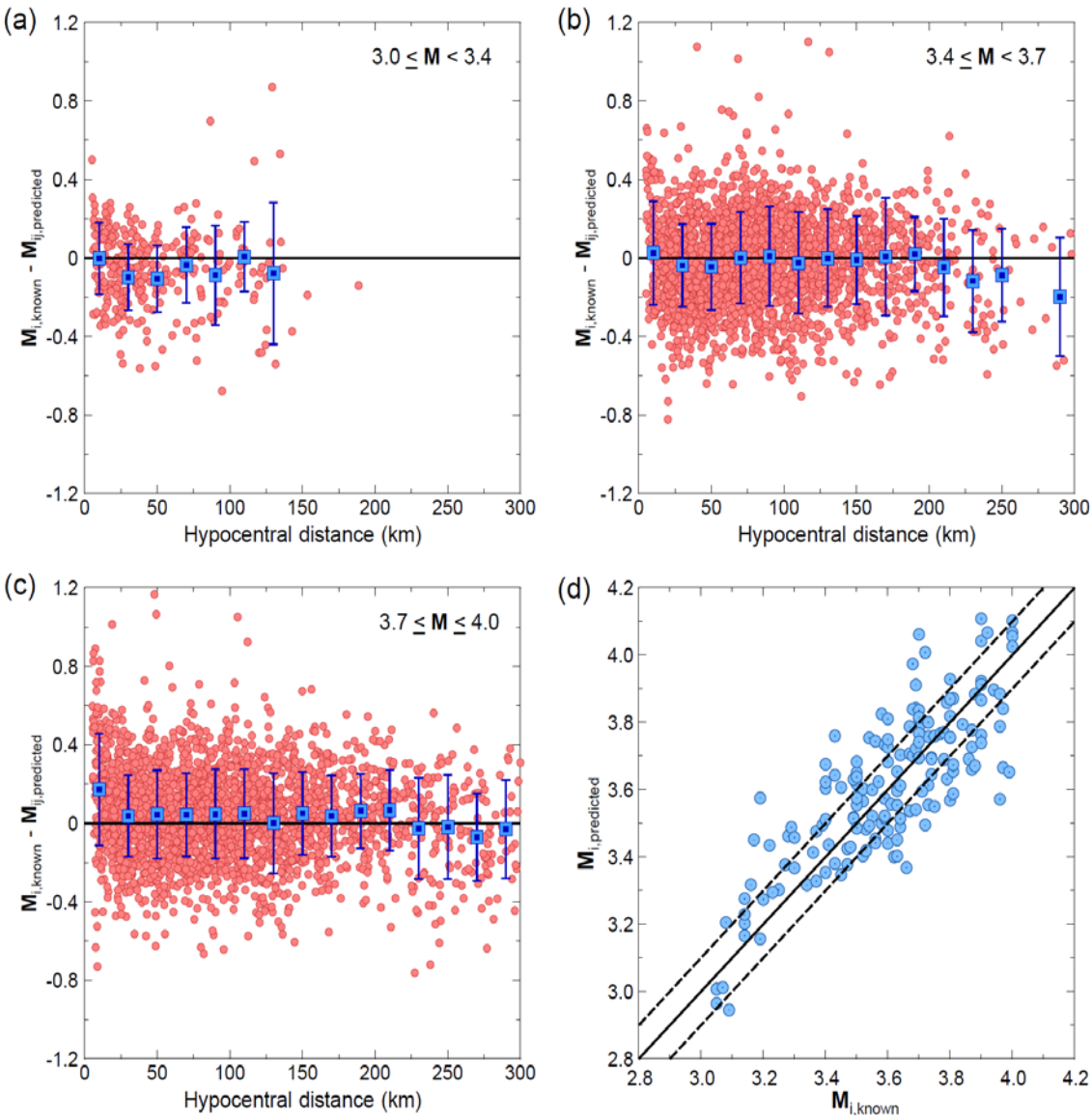

*Figure 4 – Assessment of **M** estimates (Eqn. 2) based on the ground motions from NGA-W2 database, showing **M** bias determined for each record, as a function of hypocentral distance for three magnitude ranges (a to c). Mean bias is computed over all magnitudes, at equal distance intervals of 20 km. (d) average **M** estimate and its known value for earthquakes having three or more observations at R≤300 km. The solid line represents* $\mathbf{M}_{i,predicted} = \mathbf{M}_{i,known}$ *and the dashed lines indicate ± 0.1 band about the solid line.*

We test the performance of the model for earthquakes in ENA using the NGA-East and seismotoolbox databases, as compiled by Hassani and Atkinson (2014). These data cover the regions of southeastern Canada/northeastern U.S., as well as the central U.S. (Note: tests were made to confirm that the noted trends do not differ significantly between the northeast and the central U.S.) Figure 5 shows the data amplitudes with respect to Equation 1, while Figure 6 shows the bias in terms of estimated moment magnitude, as well as average M estimates for events in the ENA database (where the **M** values are derived from, or calibrated to, regional moment tensors as in Atkinson and Babaie Mahani, 2012). The agreement is satisfactory overall, though in some magnitude ranges there is a tendency for larger-than-predicted amplitudes at close distances. However, the data at close distances are sparse. Average M estimates for earthquakes having three or more observations within 300 km are mostly within ± 0.1 units of the known **M**, for M≤4.

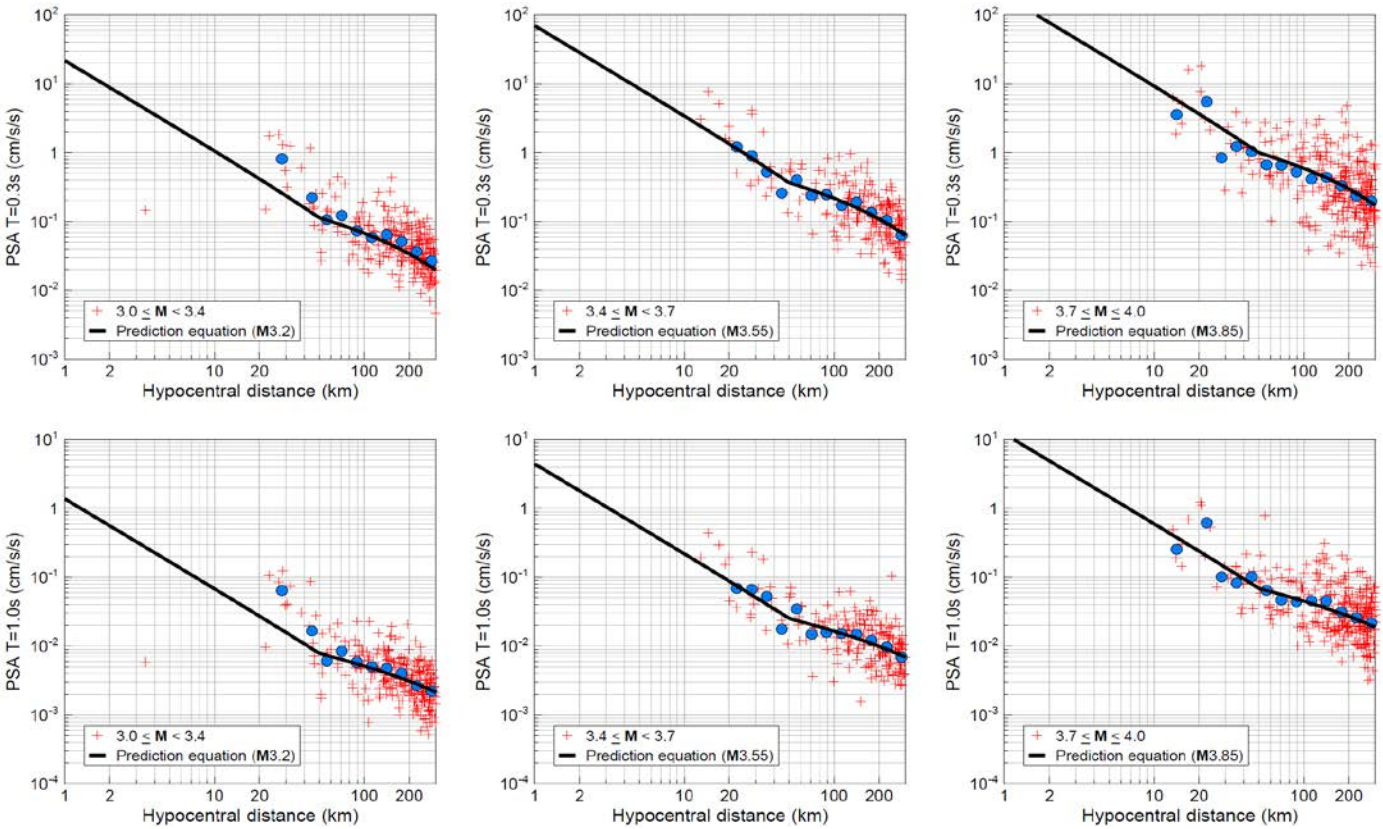

*Figure 5 – Comparison of Equation 1 (lines), evaluated at **M**=3.2, 3.55 and 3.85, with ENA ground-motion data (plus symbols), for PSA at 0.3s (top) and 1.0s (bottom). Circles show average data amplitudes in distance bins.*

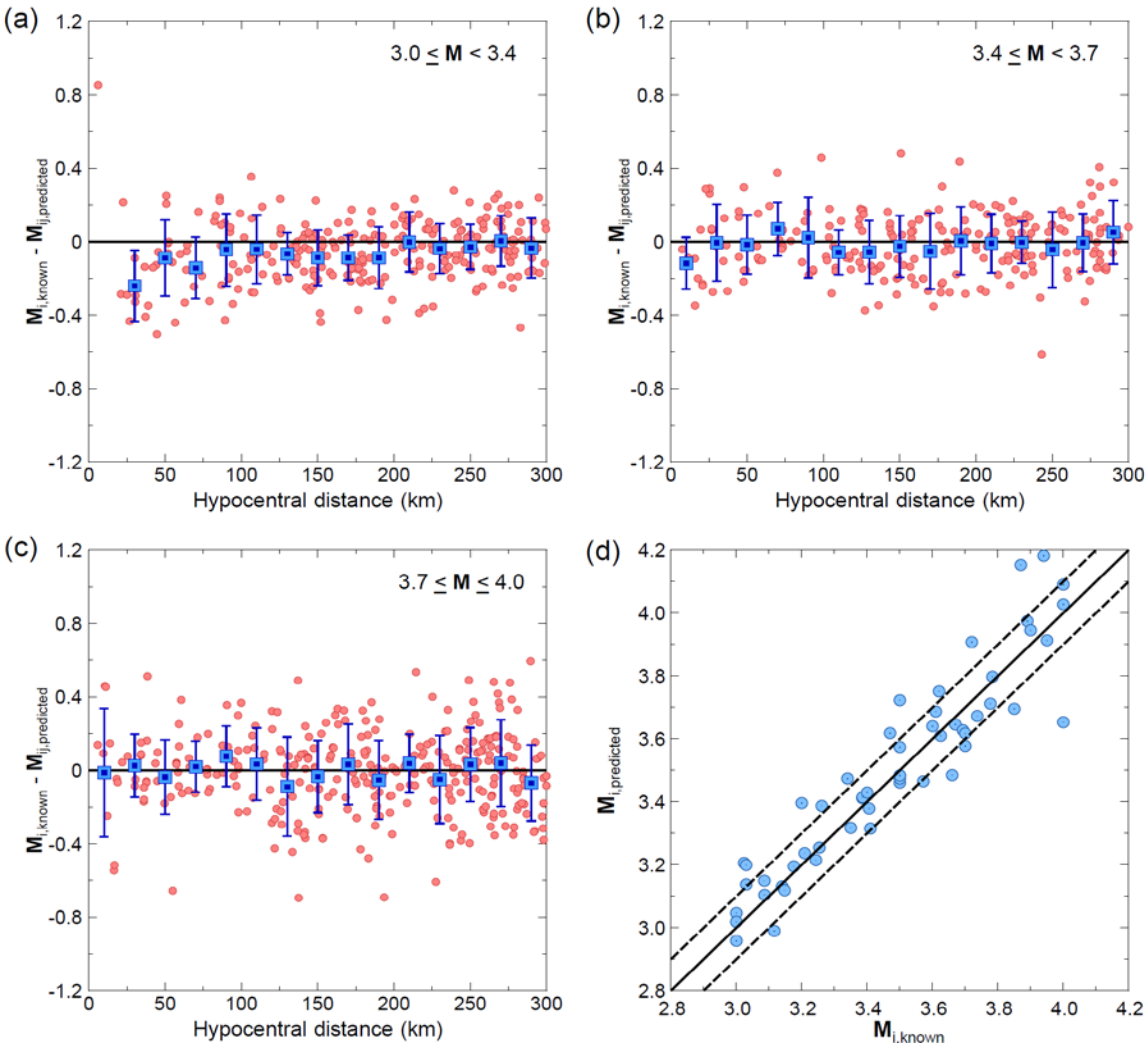

*Figure 6 – Assessment of **M** estimates (Eqn. 2) based on the ground motions from ENA database, showing **M** bias determined for each record, as a function of hypocentral distance for three magnitude ranges (a to c). Mean bias is computed over all magnitudes, at equal distance intervals of 20 km. (d) average **M** estimate and its known value for earthquakes having three or more observations at R≤300 km. The solid line represents* $\mathbf{M}_{i,predicted} = \mathbf{M}_{i,known}$ *and the dashed lines indicate ± 0.1 band about the solid line.*

Moment Magnitude Estimation for Events of M<3

We have shown that the proposed moment magnitude estimation equation based on PSA at 1s works well in both ENA and WNA, for events of **M** 3 to 4 at distances up to 300 km. The use of point-source simulations to constrain the magnitude scaling should ensure robust and meaningful magnitude estimates at smaller magnitudes. However, the influence of noise on PSA becomes important for **M**<3, and could result in a bias toward overestimation of event magnitudes. We examined typical regional network data in eastern and western Canada to determine response spectral amplitudes that would be expected from noise alone (e.g. oscillator response for a window of 30 to 60 seconds in length, in the absence of any earthquake signal). It is common to observe PSA, from noise alone, in the range from 10^{-4} to 10^{-3} cm/s^2, over a broad period band. As illustrated in Figure 7, this significantly limits the magnitude-distance range over which we can obtain moment magnitudes using PSA at 1s, because small events will only have significant signal, in relation to the noise PSA, at very close distances. One solution would be to reduce the noise through improved installation techniques, for

example by placing instruments in deep boreholes. A more economical and practical solution in most situations is to choose a period band where the signal for small events is stronger. This is the motivation for using 0.3s PSA in place of 1s PSA, for events of **M**<3, and why we derived equations using both 0.3s and 1s PSA values. Specifically, we observe in Figure 7 that for relatively-quiet conditions (the lower noise level), the signal PSA at 0.3s is above noise for events of M=1 within 40 km, whereas for 1s it is only above noise within 8 km. For events of **M**<3, the 0.3s PSA is at a sufficiently long period to represent the moment of the event (Figure 1), and thus it is logical to use the 0.3s PSA in preference to the 1s value to improve the signal-to-noise ratio.

As a practical matter, then, we propose that if the magnitude value calculated from the 1s PSA is <3, the magnitude for the event should be recalculated using the 0.3s PSA. We tested to confirm that there is no significant difference, on average, between **M** computed from 0.3s or 1s, for events in the NGA-W2 and ENA databases, for events of **M** 3 to 4, though the **M** value determined for individual events may vary by +/- 0.13 units (standard deviation) depending on which ground-motion parameter is selected. We also investigated more generally if there is an advantage to using an average of **M** from the two ground-motion parameters, for events in the intermediate-magnitude range of **M**3.0 to **M**3.5, and found that this also makes no difference – individual-event **M** values may vary slightly (+/- 0.1), but overall the bias and its variability are the same. We therefore would generally recommend using the 1s PSA formula for the initial **M** calculation, and switching to the 0.3s PSA formula if the calculated **M** from 1s PSA is less than 3.0.

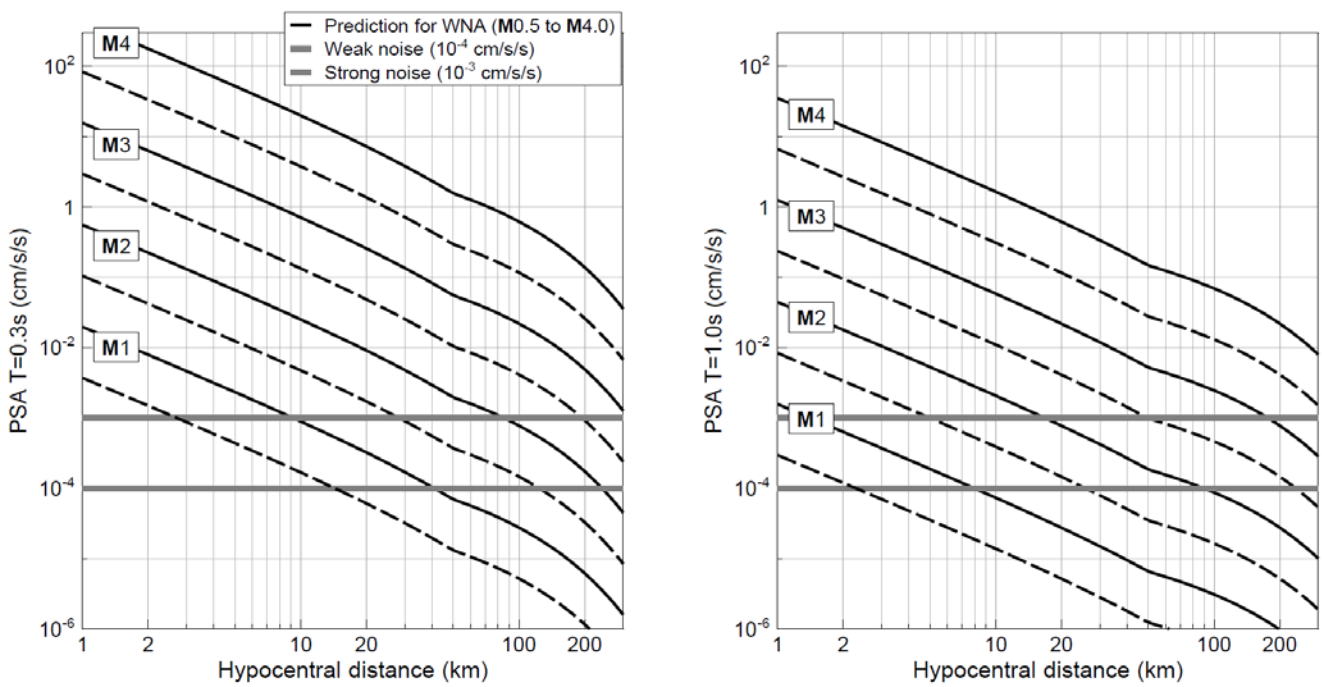

Figure 7 – Comparison of predicted PSA for WNA at 0.3s (left) and 1.0s (right) for events of M0.5 to 4.0, versus hypocentral distance (black lines). Heavy grey horizontal lines show typical weak and strong noise levels.

Ideally, we would like to be able to evaluate the performance of the algorithm for events as small as **M** 1, which is the threshold for some traffic light protocols. Small-magnitude ground-motion datasets with reliable moment magnitude estimates are difficult to obtain, but a very good set was compiled by Douglas et al. (2013). They used ground-motion data from induced events, along with stochastic simulations, to develop a GMPE for induced earthquake ground motions in geothermal areas, including several areas in Europe and California.

Their database of several thousand records contains events in the **M** 1 to 4 range, at close distances (<50 km). Douglas et al. compiled horizontal-component PSA, but corrected it for site conditions to an equivalent rock site condition, as characterized by a near-surface shear-wave velocity of 1100 m/s. Because of the correction to a reference rock condition, their horizontal-component amplitudes should be similar to those expected on the vertical component (e.g. see Siddiqqi and Atkinson, 2002). Douglas et al. (2013) analyzed displacement spectral amplitudes in order to estimate moment magnitude for all events, as based on the Brune model. Atkinson (2014) shows that the observed ground-motion amplitudes for the Douglas database are well-predicted by the stochastic simulation model for western events employed in this study. It is therefore reasonable to compare the magnitude estimation procedure proposed herein against the Douglas et al. database, assuming that the horizontal-component, corrected for site effects, is equivalent to the vertical component. The comparison is shown in Figure 8 for events recorded by three or more stations. The magnitude calculations track each other well, but the moment magnitudes calculated by our algorithm using 0.3s PSA are on average 0.14 (+/-0.20) units higher than those calculated by Douglas et al. (2013). There are many more data available in their database at 0.3s (3300 records) than at 1s (120 records), due to noise limitations, which further supports the switch to PSA at 0.3s for **M**<3 events. The agreement of average magnitude values within ~0.1 units is considered satisfactory, despite the significant variability in estimates from event-to-event. Thus we believe the moment-M algorithm is robust down to at least **M**1.5. We note on Figure 8 that there is a greater tendency toward overestimation of **M** for **M**<1.5, likely due to noise effects on PSA.

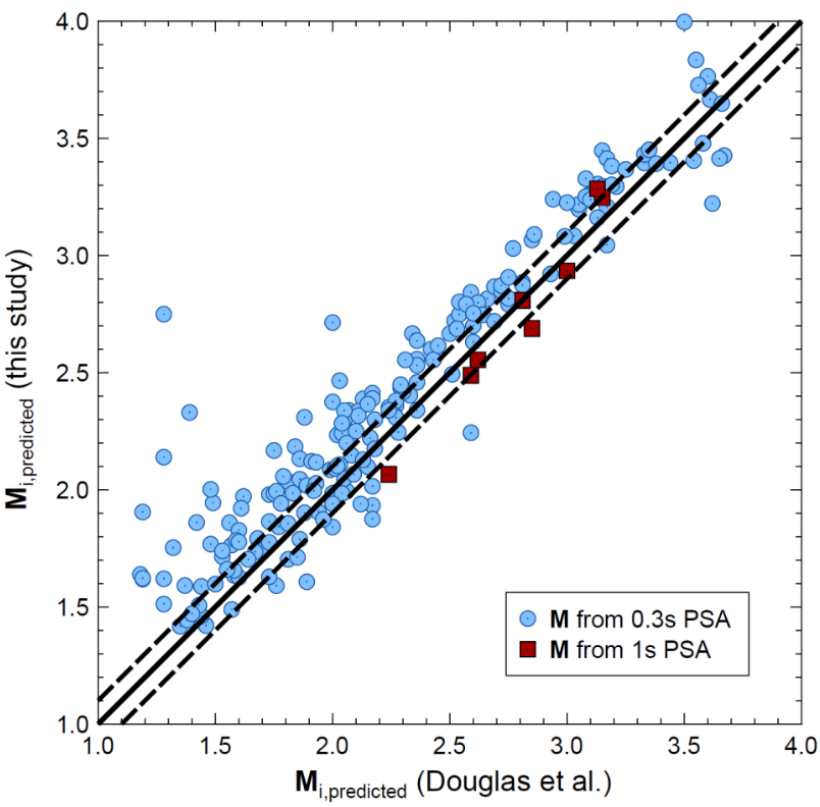

Figure 8 – Comparison of **M** *estimated from PSA (this study) to* **M** *estimated from displacement spectra, for induced-seismicity ground-motion database of Douglas et al. (2013), for events recorded by three or more stations. The heavy solid line represents one-to-one match of magnitude estimates and the dashed lines indicate ± 0.1 band about the solid line.*

For events of **M**<1.5, our ability to determine magnitude will be limited by the station distribution and noise. If there are insufficient stations with clear signal to noise ratio (e.g. a factor of 3 or more over a significant frequency band), then the best that can be accomplished is to estimate an upper limit on the actual magnitude. For example, one might calculate **M** at each of the three closest stations (even if just barely above noise), all of which should be overestimates of the actual value of **M**, and estimate an upper limit on **M** as the average of these values. This strategy may be sufficient to establish that an event did not exceed a traffic light threshold such as **M**1.

Conclusion

We have proposed a simple model (Eqn 2) to provide robust estimates of moment magnitude for events of M<4, at distances less than ~300km. The model can be refined on a regional basis as more detailed empirical information on the overall amplitude level and attenuation is gathered. The method is transparent and robust, being based on simple and well-known seismological scaling principles, and can be used in typical network applications, as well as for traffic light systems for induced seismicity.

Acknowledgements

We thank Karen Assatourians, Behzad Hassani, Arpit Singh and Sebastian Braganza for their help in compiling and processing datasets for the analyses. Financial support for this study was provided by the National Sciences and Engineering Research Council of Canada, TransAlta, and Nanometrics. We are grateful to Trevor Allen for constructive comments that improved the paper. We thank John Douglas for sharing his compiled data, and to the following for their permission to examine its components: Dirk Kraaijpoel (KNMI), Phillippe Jousset (ICGR), Vincenzo Convertito (INGV), Ben Edwards (ETHZ).

References

Anderson, J. G., and S. E. Hough (1984). A model for the shape of the Fourier amplitude spectrum of acceleration at high frequencies, Bull. Seism. Soc. Am. **74**, 1969-1993.

Atkinson, G. (2012). Evaluation of attenuation models for the northeastern U.S./Southeastern Canada. Seism. Res. L., 83, 166-178.

Atkinson, G. (2014). Ground-motion prediction equation for small-to-moderate events at short hypocentral distances, with application to induced seismicity hazards. Bull. Seism. Soc. Am., submitted.

Atkinson, G., K. Assatourians, D. Boore, K. Campbell and D. Motazedian (2009). A guide to differences between stochastic point-source and stochastic finite-fault simulations. Bull. Seism. Soc. Am., 99, 3192-3201.

Atkinson, G. and A. Babaie Mahani (2013). Estimation of moment magnitude from ground motions at regional distances. Bull. Seism. Soc. Am., 103, 107-116.

Atkinson, G. and D. Boore (2006). Ground motion prediction equations for earthquakes in eastern North America. Bull. Seism. Soc. Am., 96, 2181-2205.

Atkinson, G. and D. Boore (2014). The attenuation of Fourier amplitudes for rock sites in eastern North America. Bull. Seism. Soc. Am., **104**, 513-528.

Atkinson, G. and W. Silva (2000). Stochastic modeling of California ground motions. Bull. Seism. Soc. Am., 90, 255-274.

Babaie Mahani, A. and G. Atkinson (2012). Regional differences in ground‐motion amplitudes of small‐to‐moderate earthquake across North America. Bull. Seism. Soc. Am., 103, 2604-2620.

Boore, D. (1983). Stochastic simulation of high-frequency ground motions based on seismological models of the radiated spectra. Bull. Seism. Soc. Am., 73, 1865-1894.

Boore, D. M. (2000). SMSIM; Fortran programs for simulating ground motions from earthquakes; version 2.0, OF 00-0509, 55.

Boore, D. (2003). Prediction of ground motion using the stochastic method. Pure and Applied Geophysics, 160, 635-676.

Brune, J. (1970). Tectonic stress and the spectra of seismic shear waves from earthquakes. J. Geophys. Res., 75, 4997-5009.

Campbell, K. (2009). Estimates of shear-wave Q and κ_0 for unconsolidated and semiconsolidated sediments in Eastern North America. Bull. Seism. Soc. Am., **99**, 3192-3201.

Douglas, J., B. Edwards, V. Convertito, N. Sharma, A. Tramelli, D. Kraaijpoel, B. Mean Cabrera, N. Maercklin and C. Troise (2013). Predicting ground motion from induced earthquakes in geothermal areas. Bull. Seism. Soc. Am., **103**, 1875-1897.

Hanks, T. and H. Kanamori (1979). A moment magnitude scale. J. Geophys. Res., 84, 2348-2350.

Hassani, B. and G. Atkinson (2014). Referenced Empirical ground motion model for central and eastern North America. Seism. Res. L., in press.

Lermo, J. and F. Chavez-Garcia (1993). Site effect evaluation using spectral ratios with only one station. Bull. Seism. Soc. Am., 83, 1574-1594.

Raoof, M., R. Herrmann and L. Malagnini (1999). Attenuation and excitation of three-component ground motion in sourthern California. Bull.Seism. Soc. Am., 89, 888-902.

Siddiqqi, J. and G. Atkinson (2002). Ground motion amplification at rock sites across Canada, as determined from the horizontal-to-vertical component ratio. Bull. Seism. Soc. Am., 92, 877-884.

Wald, D.J., Quitoriano, V., Heaton, T.H., Kanamori, H., Scrivner, C.W. and Worden, B.C., 1999c, TriNet "ShakeMaps": Rapid generation of peak ground-motion and intensity maps for earthquakes in southern California. Earthquake Spectra, **15**, 537-556.

Yenier, E and G. Atkinson (2014). Equivalent point-source modeling of moderate- to-large magnitude earthquakes and associated ground-motion saturation effects, Bull. Seism. Soc. Am. 104, (in press).

3 - Regionally-Adjustable Generic Ground-Motion Prediction Equation based on Equivalent Point-Source Simulations:

Application to Central and Eastern North America

(Emrah Yenier and Gail M. Atkinson, submitted to Bull. Seism. Soc. Am., Nov. 2014)

Section Summary

We develop a generic ground-motion prediction equation (GMPE) that can be adjusted for use in any region by modifying a few key model parameters. The basis of the GMPE is an equivalent point-source simulation model whose parameters have been calibrated to empirical data in California, in such a way as to determine the decoupled effects of basic source and attenuation parameters on ground motion amplitudes. We formulate the generic GMPE as a function of magnitude, distance, stress parameter, geometrical spreading rate and anelastic attenuation coefficient. This provides a fully adjustable predictive model, allowing users to calibrate its parameters using observed motions in the target region. We also include an empirical calibration factor to account for residual effects that are different and/or missing in simulations compared to observed motions in the target region. As an example application, we show how the generic GMPE can be adjusted for use in central and eastern North America (CENA), and calibrated with the NGA-East database. We provide median predictions of ground motions in CENA for average horizontal-component peak ground motions and 5%-damped pseudo spectral acceleration (periods up to T = 10 s), for magnitudes **M**3 to **M**8 and distance up to 600 km.

Introduction

Reliable estimates of ground motions that may be produced by future earthquakes require robust modeling of the earthquake source and attenuation attributes in the region of interest. Ground-motion observations from past events provide a valuable empirical basis to develop ground-motion prediction equations (GMPEs) that describe amplitudes as a function of variables such as magnitude, distance and site condition. However, with the exception of well-monitored active regions such as California and Japan, empirical ground-motion data are generally sparse in the magnitude-distance range of engineering interest. Thus there are insufficient data for development of reliable GMPEs in many regions, with central and eastern North America (CENA) being a classic example.

There are several alternative methods used for derivation of GMPEs in data-poor regions. A widely-used method is the simulation-based approach, in which synthetic ground motions are generated over a wide magnitude and distance range, and the GMPE is developed based on the simulated amplitude data. The simulations are based on a seismological model of the source, path and site effects, with the parameters being calibrated using the available empirical data for the region. Simulations can be performed using a variety of techniques ranging from simple stochastic point-source methods to more sophisticated finite-source broadband simulations (e.g., Atkinson and Boore, 1995, 2006; Toro et al., 1997; Silva et al., 2002; Somerville et al., 2001, 2009; Frankel, 2009). Another common approach is the hybrid empirical method (Campbell, 2002, 2003). This method calibrates an empirically well-constrained GMPE in a data-rich host region (e.g., western North America, WNA) for use in a data-poor target region (e.g., CENA) based on adjustment factors obtained from response-spectral ratios of stochastic simulations in the host and target regions (e.g., Campbell, 2002, 2003; Scherbaum et al., 2005; Pezeshk et al., 2011). A third method is the referenced empirical approach introduced by Atkinson, (2008). It is similar to the hybrid empirical method in concept but adjustment factors are

determined empirically using spectral ratios of observed motions in the target region to predictions of an empirical GMPE in the host region (e.g., Atkinson, 2008, 2010; Atkinson and Boore, 2011, Atkinson and Motazedian, 2013; Hassani and Atkinson, 2014).

Both the hybrid empirical method and the referenced empirical approach anchor their predictions to magnitude scaling and saturation effects observed in data-rich regions, assuming that these effects are transferable. Although the magnitude scaling is assumed to be similar between regions, no such assumption is made regarding the overall level of ground-motion amplitudes. Differences in overall amplitude level and distance scaling between regions are attributed to regional differences in fundamental source and attenuation parameters. The hybrid empirical method requires sound knowledge of these parameters in both host and target regions in order to determine host-to-target adjustment factors via simulations reliably. This may restrict the applicability of the method (Campbell, 2003). The referenced empirical approach resolves this issue by determining the adjustment factors empirically, avoiding the need for assumptions of the source and attenuation parameters for the host and target regions. An important limitation of the referenced empirical approach, however, is that the available ground-motion data in the target region may not sufficiently represent all important regional characteristics (Atkinson, 2008).

In this study, we take advantage of key concepts from both the hybrid empirical and referenced empirical approaches to develop a robust simulation-based generic GMPE. The generic GMPE can be adjusted for use in any region by modifying a few key modeling parameters, and calibrated for regional use from limited empirical data. The basic idea is that we first develop a well-calibrated simulation-based GMPE for active tectonic regions, using the NGA-West2 database (Ancheta et al., 2014). We parameterize this generic GMPE so as to isolate the effects of the basic source and attenuation parameters on peak ground motions and response spectra. This provides effective and transparent control over the transferable factors between regions. The fundamental seismological parameters that are used as predictive variables in the generic GMPE include magnitude, distance, stress parameter, geometrical spreading rate and the anelastic attenuation coefficient. This provides an adjustable predictive model that is readily calibrated with minimal regional data. In the generic GMPE, we also consider an empirical calibration factor to account for residual effects that are different and/or missing in simulations compared to empirical data. This closes any remaining gap between simulated and observed motions.

As an example implementation of the generic model, we use it to develop a GMPE for CENA by adjusting the stress and anelastic attenuation, and calibrate the model using the NGA-East database. During the calibration exercise, we infer a magnitude- and depth-dependent stress parameter model based on the values obtained from study events. We provide median predictions of ground motions in CENA for average horizontal-component peak ground motions and 5%-damped pseudo spectral acceleration (periods up to T = 10 s), for wide ranges of magnitude (**M**3-**M**8) and distance (< 600 km).

Functional Form of the Generic GMPE

A regionally-adjustable generic prediction equation requires a robust yet simple functional form that successfully decouples the effects of fundamental source and attenuation parameters on ground-motion amplitudes. We define the generic GMPE as

$$\ln Y = F_E + F_Z + F_\gamma + F_S + C \qquad (1)$$

where $\ln Y$ is the natural logarithm of a ground-motion intensity measure. F_E, F_Z, F_γ and F_S represent functions for earthquake source, geometrical spreading, anelastic attenuation and site effects, respectively. The C term is

an empirical calibration factor that accounts for the residual differences between simulations and empirical data. We formulate the source and geometrical spreading effects (F_E and F_Z) in an equivalent point-source sense, using ground-motion simulations with parameters calibrated to observations in California, obtained from the NGA-West2 database (Ancheta et al., 2014). The anelastic attenuation (F_γ) is adjusted to optimize observed frequency-dependent attenuation effects. In this study, we provide predictions for the orientation-independent horizontal component of peak ground acceleration (PGA), peak ground velocity (PGV) and 5%-damped pseudo-spectral acceleration (PSA), where PGA and PSA are given in units of *g* and PGV is in cm/s.

The source function (F_E) describes the effects of magnitude and stress parameter on ground-motion amplitudes as:

$$F_E = F_M + F_{\Delta\sigma} \tag{2}$$

where F_M represents the ground motions (for moment magnitude **M)** that would be observed at the source, if there were no distance-saturation effects, for the reference stress ($\Delta\sigma$) and kappa (κ_0) parameters, for the reference site condition. We choose $\Delta\sigma$ = 100 bar and κ_0 = 0.025 s as the reference modeling parameters based on the findings of Yenier and Atkinson (2014b) for California earthquakes. In Equation 2, $F_{\Delta\sigma}$ represents the stress adjustment factor that is needed when $\Delta\sigma$ is different than 100 bars.

The F_M term is defined as a function of moment magnitude (**M**), using a hinged-quadratic function:

$$F_M = \begin{cases} e_0 + e_1(\mathbf{M} - \mathbf{M}_\mathrm{h}) + e_2(\mathbf{M} - \mathbf{M}_\mathrm{h})^2 & \mathbf{M} \le \mathbf{M}_\mathrm{h} \\ e_0 + e_3(\mathbf{M} - \mathbf{M}_\mathrm{h}) & \mathbf{M} > \mathbf{M}_\mathrm{h} \end{cases} \tag{3}$$

where the hinge magnitude, $\mathbf{M}_\mathrm{h}$, and model coefficients, e_0 to e_3, are period-dependent. This mimics the functional form of magnitude scaling used by Boore et al. (2014) in their NGA-West2 empirical GMPE.

The stress adjustment term is defined as:

$$F_{\Delta\sigma} = e_{\Delta\sigma}\ln(\Delta\sigma/100) \tag{4}$$

where $e_{\Delta\sigma}$ describes the rate of the ground-motion scaling with $\Delta\sigma$. Equation 4 describes the relationship between stress parameter and response spectral amplitudes, facilitating the determination of $\Delta\sigma$ from PSA data in the target region.

We model the geometrical spreading effects based on the equivalent point-source method. Seismic waves are assumed to radiate from a virtual point source placed at an overall effective distance from the site, such that the empirically-observed saturation effects are successfully reproduced. The effective distance (*R*) is given as

$$R = \sqrt{{D_{rup}}^2 + h^2} \tag{5}$$

where D_{rup} is the closest distance from the site to the fault-rupture surface and *h* is a pseudo-depth term that accounts for distance saturation effects. The pseudo-depth is generally defined as a function of magnitude to account for the extension of distance-saturation effects to larger distances with increasing magnitude. In this study, we define the pseudo-depth as

$$h = 10^{-0.405 + 0.235\mathbf{M}} \tag{6}$$

Equation 6 is defined from a loose interpretation of the findings of recent empirical studies, as shown in Figure 1, in such a way as to preclude oversaturation of predicted amplitudes at large magnitudes (shown later).

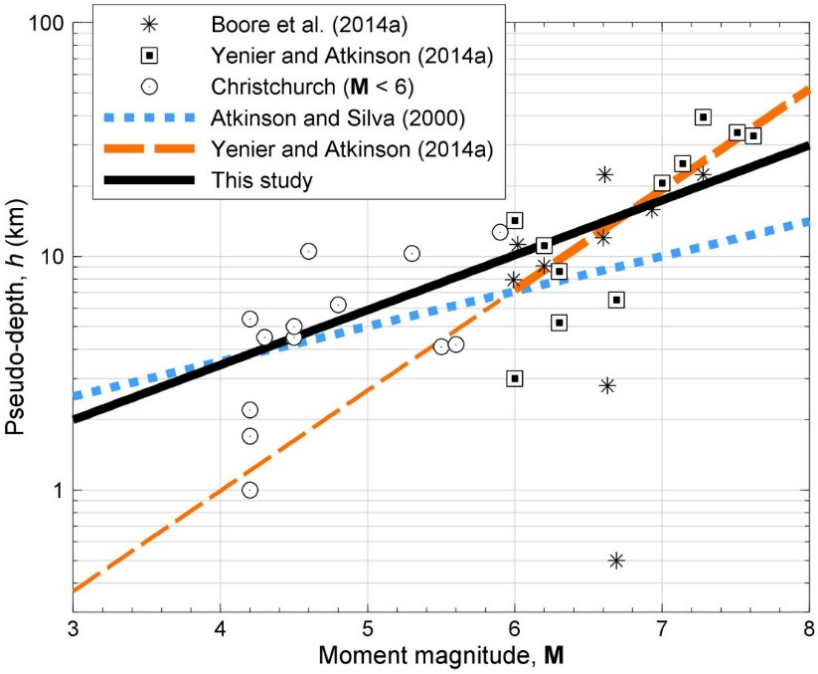

Figure 1. *Pseudo-depths (h) determined from modeling of observed ground motion (symbols) and alternative pseudo-depth models (lines). Asterisks and squares indicate h values obtained from well-recorded earthquakes of* ***M*** *≥ 6 around the world by Boore et al. (2014a) and Yenier and Atkinson (2014a), respectively. Circles represent h values calculated from the modeling of the 2010-2012 Christchurch, New Zealand aftershocks of* ***M*** *< 6 (Yenier and Atkinson, manuscript in preparation). The relations proposed by Atkinson and Silva (2000) and Yenier and Atkinson (2014a) are shown by heavy dotted and dashed lines, respectively. The thin dashed line indicates the extrapolation of Yenier and Atkinson (2014a) model for* ***M*** *< 6. The h model used in this study (Equation 6) is shown by the heavy solid line.*

We define the geometrical spreading function (F_Z) as

$$F_Z = \ln(Z) + (b_3 + b_4\mathbf{M}) \ln\left(R/R_{ref}\right) \tag{7}$$

where Z represents the geometrical attenuation of Fourier amplitudes, while the multiplicative component, $(b_3+b_4\mathbf{M})\ln(R/R_{ref})$, accounts for the change in the apparent attenuation that occurs when ground motions are modeled in the response spectral domain rather than the Fourier domain. The coefficients b_3 and b_4 are period-dependent, and R_{ref} is the reference effective distance, given as $R_{ref} = \sqrt{1 + h^2}$.

In ground-motion modeling, Z is generally considered as a piecewise continuous function that describes the distance-dependent attributes of geometrical spreading, considering the contributions of direct waves at close distances, and multiple reflections and refractions at larger distances. Babaie Mahani and Atkinson (2012) evaluated the ability of various functional forms to describe the geometrical attenuation in North America, and concluded that a bilinear model provides a good balance between simplicity and ability to capture the key attenuation attributes over a broad distance range. In this study, we define Z using a hinged bilinear model that provides for a transition from direct-wave spreading to surface-wave spreading of reflected and refracted waves:

$$Z = \begin{cases} R^{b_1} & R \le R_t \\ {R_t}^{b_1}(R/R_t)^{b_2} & R > R_t \end{cases} \tag{8}$$

where R_t represents the transition distance, and b_1 and b_2 are the geometrical attenuation rates of Fourier amplitudes at $R \leq R_t$ and $R > R_t$, respectively. In the generic GMPE, we fix the transition distance at R_t = 50 km based on the findings of Yenier and Atkinson (2014a).

The geometrical spreading rate at close distances is often assumed to be given by b_1 = -1.0, based on the homogeneous whole-space approximation. However, theoretical waveform simulations suggest faster spreading rates, about $b_1 \approx$ -1.3, for typical layered earth models (Ojo and Mereu 1986; Burger et al., 1987; Ou and Herrmann, 1990; Somerville et al., 1990; Chapman and Godbee, 2012, Chapman 2013). Empirical modeling of ground motions in various regions, including WNA, CENA and Australia also support this finding (Atkinson, 2004; Allen, 2007; Babaie Mahani and Atkinson, 2012; Yenier and Atkinson, 2014a, 2014b). Therefore, we define the geometrical spreading rate at $R \leq 50$ km as b_1 = -1.3 in the generic model. The geometrical spreading rate at $R > 50$ km is fixed at the widely-used value of b_2 = -0.5, which is consistent with attenuation of surface waves in a half-space (Ou and Herrmann 1990; Atkinson 2012).

Equation 7 effectively decouples the geometrical spreading of Fourier amplitudes (Z) and the change in observed decay of amplitudes when convolved by the response transfer function. Although the descriptive parameters of Z are fixed at their generic values in the model, Equation 7 allows modification of the shape and rates of Z if there is compelling evidence supporting such a change. In such a case, the preferred model as given in Equation 8 can be replaced with an alternative geometrical spreading model that is compatible with the decay of the Fourier amplitudes in the target region.

The anelastic attenuation function (F_γ) is given as:

$$F_\gamma = \gamma D_{rup} \tag{9}$$

where γ is a period-dependent anelastic attenuation coefficient that is empirically determined from regional ground-motion data.

In the generic GMPE, we describe site effects relative to a reference condition of NEHRP (National Earthquake Hazards Reduction Program) B/C boundary, for which the travel-time weighted average shear-wave velocity over the top 30 m is V_{S30} = 760 m/s. In this study, we adopt the site effects model of BSSA14 (Boore et al., 2014b):

$$F_S = F_{lin} + F_{nl} \tag{10}$$

where F_{lin} represents the linear site effects, and F_{nl} represents the nonlinear site effects. The linear site response is defined as a function of V_{S30}:

$$F_{lin} = \begin{cases} c\ \ln(V_{S30}/760) & V_{S30} \leq V_c \\ c\ \ln(V_c/760) & V_{S30} > V_c \end{cases} \tag{11}$$

where c describes the V_{S30}-scaling and V_c is the limiting velocity beyond which ground motions no longer scale with V_{S30}. The nonlinear site response is given as

$$F_{nl} = f_1 + f_2 \ln\left[\frac{PGA_r + f_3}{f_3}\right] \tag{12}$$

where f_2 represents the degree of nonlinearity as a function of V_{S30}:

$$f_2 = f_4[\exp\{f_5(\min(V_{S30}, 760) - 360)\} - \exp\{f_5(760 - 360)\}] \tag{13}$$

In Equations 11 to 13, parameters c, V_c, f_1, f_3, f_4 and f_5 are model coefficients given in BSSA14 and PGA_r is the median peak horizontal acceleration predicted for the reference condition (V_{S30} = 760 m/s).

Determination of Model Coefficients

We calculate model coefficients of the magnitude effect (F_M), geometrical spreading function (F_Z) and stress adjustment factor ($F_{\Delta\sigma}$) from amplitude data generated from ground-motion simulations. The simulations are based on the equivalent point-source stochastic method with modeling parameters calibrated to observed motions in California as described by Yenier and Atkinson (2014b); model parameters are summarized in Table 1. Briefly, we use the additive double-corner-frequency source model of Boore et al. (2014a) with a spectral-sag parameter (ε) suggested by Yenier and Atkinson (2014b). In simulations, the geometrical decay of Fourier amplitudes (Z) is defined in terms of effective distance, as given in Equation 8 (b_1 = -1.3, b_2 = -0.5 and R_t = 50 km). We use the pseudo-depth model given in Equation 6 to account for near-distance saturation effects. We constrained the pseudo-depth function to avoid oversaturation of predicted amplitudes at large magnitudes, which is why this function is slightly different than the h model used in Yenier and Atkinson (2014b). The simulations do not include anelastic attenuation, because we will determine these effects empirically from regional ground-motion data (shown later). We simulate ground motions at NEHRP B/C site conditions assuming the generic crustal amplification factors given by Atkinson and Boore (2006). We assume that the near-surface high-frequency attenuation parameter is κ_0 = 0.025 s for this site class. Yenier and Atkinson (2014b) showed that equivalent point-source simulations with these modeling parameters (but also including regional anelastic attenuation effects) can reproduce average observed spectral amplitudes of earthquakes in California, for magnitudes up to **M**7.5 and distances less than 400 km. Any inadequacies or misfits between the simulations and empirical data will map into unresolved residuals, which will be taken into account through the calibration factor, C.

Table 1. *Parameter values used in stochastic equivalent point-source simulations (from Yenier and Atkinson, 2014b)*

Parameter	Value
Shear-wave velocity	β = 3.7 km/s
Density	ρ = 2.8 g/cm^3
Source model	Generalized additive double-corner-frequency source model of Boore et al. (2014a)
Spectral sag	$\varepsilon = min[1, 10^{1.2 - 0.3\mathbf{M}}]$
Effective distance	$R = (D_{rup}^2 + h^2)^{0.5}$
Pseudo-depth	$h = 10^{-0.405 + 0.235\mathbf{M}}$
Geometrical attenuation	$R^{-1.3}$ for $R \leq 50$ km, and $50^{-1.3}(R/50)^{-0.5}$ for $R > 50$ km
Anelastic attenuation	Not considered in simulations (determined empirically)

Site amplification (NEHRP B/C)	Table 4 of Atkinson and Boore (2006) Frequency-amplification pairs delimited by semicolons: 0.0001Hz-1; 0.1Hz-1.07; 0.24Hz-1.15; 0.45Hz-1.24; 0.79Hz-1.39; 1.38Hz-1.67; 1.93Hz-1.88; 2.85Hz-2.08; 4.03Hz-2.2; 6.34Hz-2.31; 12.5Hz-2.41; 21.2Hz-2.45; 33.4Hz-2.47; 82Hz-2.50
Kappa factor	κ_0 = 0.025 s
Source duration	$0.5/f_a + 0.5/f_b$ where f_a and f_b are the corner frequencies
Path duration*	Table 1 of Boore and Thompson (2014) Rupture distance-path duration pairs delimited by semicolons: 0km-0s; 6.59km-2.32s; 44.7km-8.32s; 124.8km-10.9s; 175km-17.5s; 269km-34.1s. Path duration increases with distance at a rate of 0.156s/km after the last nodal point.
Simulation calibration factor for California†	C_{sim} = 3.16

* The nodal rupture distances of Boore and Thompson (2014) are converted to effective distance using the pseudo depths (h) for each magnitude level.

† Factor applied to simulations for matching simulations to observed response spectra in California with zero bias. (Reader is referred to Yenier and Atkinson (2014b) for more information regarding the C_{sim} parameter)

We perform time-domain equivalent point-source stochastic simulations using the widely-cited SMSIM software (Boore, 2003, 2005), for magnitudes from **M**3 to **M**8 (with increments of 0.1 **M** units) and distances from 1 km to 400 km (with increments of 0.1 $\log_{10}$ units), for a fixed stress parameter of $\Delta\sigma$ = 100 bar. We generate 100 synthetic ground motions for each combination of **M**, D_{rup}. For each simulated time series we calculate PGA, PGV and PSA at 31 periods from 0.01 s to 10 s, then take the geometric mean for each parameter over the 100 simulations.

The coefficients of the magnitude-scaling term F_M are computed from the regression of simulations obtained at D_{rup} = 1 km ($Y_{\mathrm{sim,1km}}$). Recall that F_M represents the magnitude scaling of ground motions that would be observed at the source if there were no saturation effects. Therefore, we need to remove the saturation effects that we imposed in the simulations at 1km to extract the unsaturated magnitude effects, F_M. This is easily done:

$$\ln Y_{\mathrm{sim,1km}} = F_M - 1.3\ln\left(\sqrt{1+h^2}\right) \tag{14}$$

where the last term accounts for the saturation effects imposed in the simulations (i.e. F_Z at D_{rup} = 1 km). We use a grid search to determine the hinge magnitude ($\mathbf{M}_{\mathrm{h}}$), where we determine the coefficients e_0 to e_3 by regression of the amplitudes at 1 km, for each trial value of $\mathbf{M}_{\mathrm{h}}$. We select the best-fitting $\mathbf{M}_{\mathrm{h}}$ and the associated coefficients (e_0 to e_3) based on minimizing the residuals of the simulated amplitudes with respect to the model equation. Figure 2 compares ground motions simulated at D_{rup} = 1 km and the fitted model (Equation 14) as a function of magnitude, for peak ground motions and response spectra. As seen in the figure, the fitted functional form captures the magnitude scaling and saturation effects implied by simulations very well.

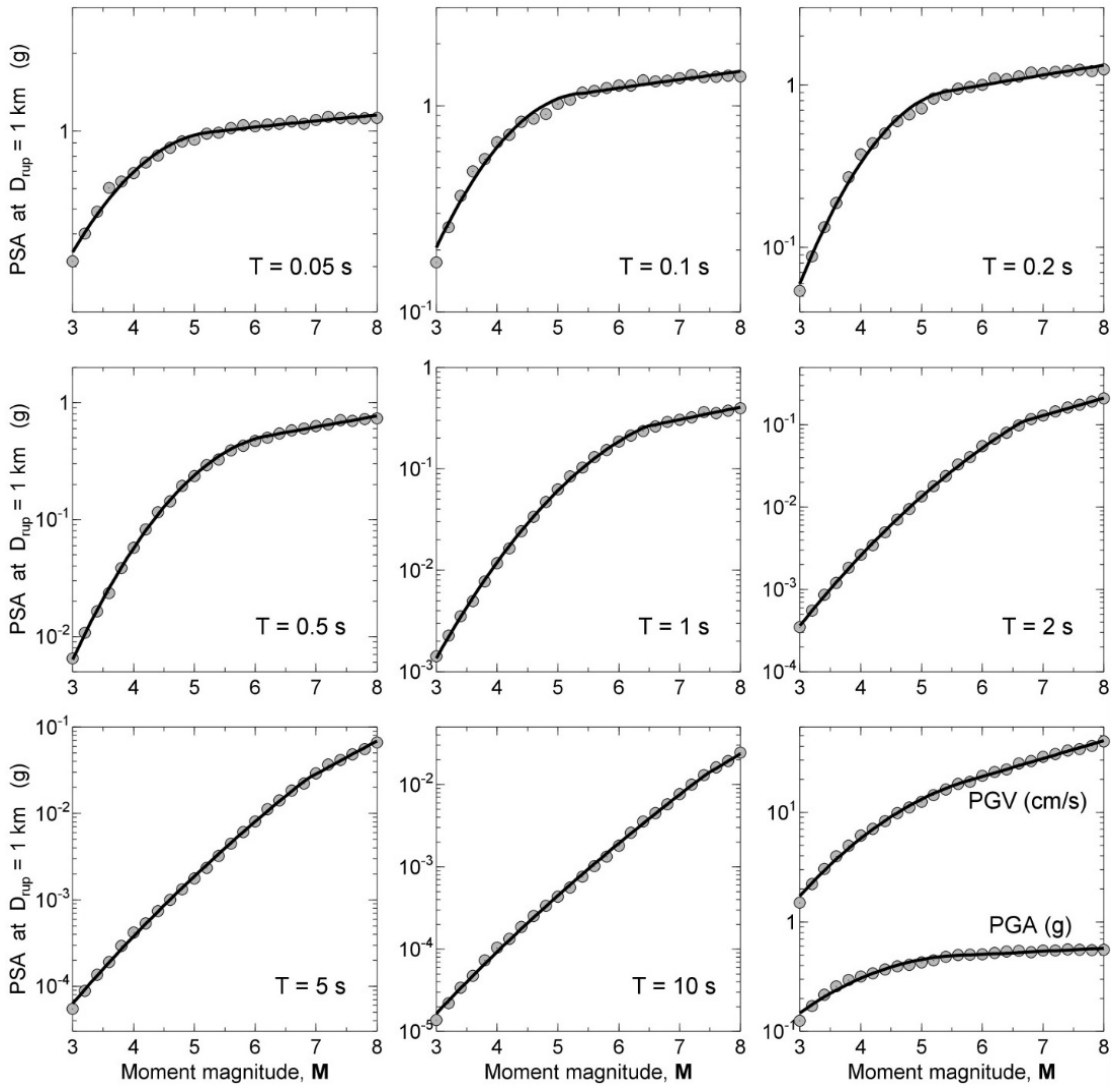

Figure 2. *Ground motions simulated at D_{rup} = 1 km (circles), and the fitted model (lines) as a function of magnitude.*

We determined the model coefficients of the geometrical spreading function from regression of simulated amplitudes at variable distances, after playing back the magnitude effects (i.e. $\ln Y_{\text{sim}} - F_M$). We use the form:

$$\ln Y_{\text{sim}} - F_M = \ln(Z) + (b_3 + b_4\mathbf{M}) \ln\left(R/R_{ref}\right) \tag{15}$$

In this regression, we constrain the Z to the decay shape used in the simulations (i.e., b_1 = -1.3, b_2 = -0.5 and R_t = 50 km). This forces the differences between the decay rates of Fourier and response spectral amplitudes to map into $(b_3+b_4\mathbf{M})\ln(R/R_{ref})$. In Figure 3, we compare the generic GMPE (i.e., $F_M + F_Z$) against simulations to assess the performance of the fitted F_Z model. This shows that the generic GMPE is in good agreement with the behavior of the simulated amplitudes. The values of model coefficients for F_M and F_Z are listed in Table 2. This specifies the generic GMPE for California for the reference stress parameter (100 bars) and the reference site condition (B/C), but without anelastic attenuation or overall amplitude calibration factor. These factors can be determined empirically, as described further later, and are listed in Table 4 for completeness.

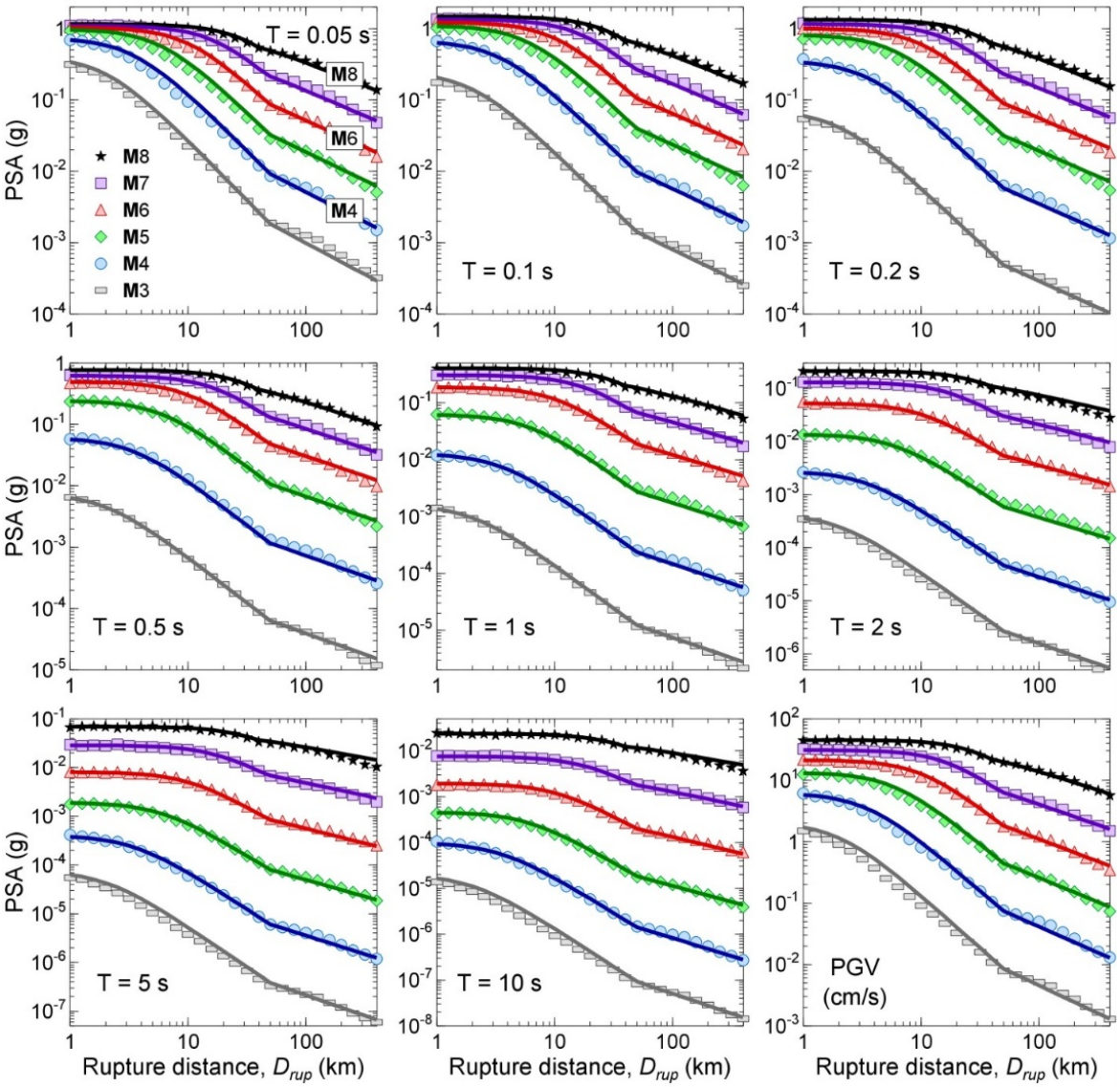

Figure 3. *Simulations (symbols) in comparison to predictions of the generic GMPE (lines), as a function of rupture distance, for magnitudes* ***M****3 to* ***M****8 (Δσ = 100 bar, V_{S30} = 760 m/s). Note that no anelastic attenuation is included in either simulations or the generic GMPE because this effect is determined empirically.*

Table 2. *Model coefficients of the magnitude term (F_M) and geometrical spreading function (F_Z) in the generic GMPE.*

T (s)	$\mathbf{M}_h$	e_0	e_1	e_2	e_3	b_3	b_4
0.010	5.85	2.23E+0	6.87E-1	-1.36E-1	7.64E-1	-6.21E-1	6.06E-2
0.013	5.90	2.28E+0	6.85E-1	-1.29E-1	7.62E-1	-6.26E-1	6.13E-2
0.016	5.85	2.27E+0	6.97E-1	-1.23E-1	7.59E-1	-6.31E-1	6.19E-2
0.020	5.90	2.38E+0	7.00E-1	-1.07E-1	7.49E-1	-6.38E-1	6.25E-2
0.025	6.00	2.56E+0	6.84E-1	-9.42E-2	7.41E-1	-6.31E-1	6.10E-2
0.030	6.15	2.81E+0	6.61E-1	-9.09E-2	7.39E-1	-6.03E-1	5.64E-2
0.040	5.75	2.73E+0	7.03E-1	-1.09E-1	7.38E-1	-5.48E-1	4.82E-2
0.050	5.35	2.56E+0	7.19E-1	-1.64E-1	7.54E-1	-5.10E-1	4.28E-2

0.065	5.75	3.00E+0	6.84E-1	-1.55E-1	7.55E-1	-4.67E-1	3.64E-2
0.080	5.20	2.58E+0	7.65E-1	-2.43E-1	7.87E-1	-4.21E-1	3.07E-2
0.100	5.45	2.78E+0	7.12E-1	-2.62E-1	7.94E-1	-3.77E-1	2.47E-2
0.130	5.35	2.64E+0	7.35E-1	-3.32E-1	8.12E-1	-3.55E-1	2.22E-2
0.160	5.25	2.47E+0	8.09E-1	-3.87E-1	8.41E-1	-3.26E-1	1.92E-2
0.200	5.45	2.55E+0	8.19E-1	-3.86E-1	8.43E-1	-2.87E-1	1.38E-2
0.250	5.60	2.52E+0	8.67E-1	-3.77E-1	8.78E-1	-2.43E-1	9.21E-3
0.300	5.85	2.63E+0	8.47E-1	-3.63E-1	8.76E-1	-2.12E-1	5.16E-3
0.400	6.15	2.67E+0	8.50E-1	-3.47E-1	8.97E-1	-1.93E-1	4.85E-3
0.500	6.25	2.54E+0	8.86E-1	-3.49E-1	9.18E-1	-2.08E-1	8.54E-3
0.650	6.60	2.62E+0	8.76E-1	-3.16E-1	9.25E-1	-2.28E-1	1.37E-2
0.800	6.85	2.66E+0	9.05E-1	-2.89E-1	8.94E-1	-2.52E-1	1.91E-2
1.000	6.45	1.99E+0	1.34E+0	-2.46E-1	9.83E-1	-2.97E-1	2.76E-2
1.300	6.75	2.01E+0	1.39E+0	-2.06E-1	1.00E+0	-3.50E-1	3.78E-2
1.600	6.75	1.75E+0	1.56E+0	-1.68E-1	1.05E+0	-3.85E-1	4.43E-2
2.000	6.65	1.25E+0	1.75E+0	-1.32E-1	1.19E+0	-4.35E-1	5.36E-2
2.500	6.70	9.31E-1	1.82E+0	-1.09E-1	1.29E+0	-4.79E-1	6.14E-2
3.000	6.65	5.16E-1	1.91E+0	-8.98E-2	1.42E+0	-5.13E-1	6.76E-2
4.000	6.85	3.44E-1	1.93E+0	-7.47E-2	1.51E+0	-5.51E-1	7.43E-2
5.000	6.85	-7.92E-2	1.98E+0	-6.21E-2	1.59E+0	-5.80E-1	7.90E-2
6.500	7.15	-6.67E-3	1.97E+0	-5.45E-2	1.63E+0	-5.96E-1	8.12E-2
8.000	7.50	2.56E-1	1.94E+0	-5.23E-2	1.59E+0	-6.09E-1	8.30E-2
10.000	7.45	-2.76E-1	1.97E+0	-4.63E-2	1.72E+0	-6.20E-1	8.42E-2
PGA	5.85	2.22E+0	6.86E-1	-1.39E-1	7.66E-1	-6.19E-1	6.03E-2
PGV	5.90	5.96E+0	1.03E+0	-1.65E-1	1.08E+0	-5.79E-1	5.74E-2

We generate another set of simulations to calculate the stress adjustment factor. In this new set, we simulate ground motions for the same magnitude range (**M**3-**M**8) but for a fixed distance D_{rup} = 1 km and variable stress parameters (10 bar ≤ Δσ ≤ 1000 bar). Similar to the first set, 100 synthetic motions are generated for each combination of **M**, D_{rup} and Δσ, and the geometric mean of the peak motions and response spectra are calculated.

The stress adjustment factor, $F_{\Delta\sigma}$, models the expected change in amplitudes when Δσ is different than 100 bars. We determine $F_{\Delta\sigma}$ using simulations obtained at D_{rup} = 1 km, as:

$$F_{\Delta\sigma} = \ln Y_{\mathrm{sim,1km}}(\mathbf{M}, \Delta\sigma) - \ln Y_{\mathrm{sim,1km}}(\mathbf{M}, 100\mathrm{bar}) \tag{16}$$

where $Y_{\mathrm{sim,1km}}(\mathbf{M},\Delta\sigma)$ is the ground motion simulated at D_{rup} = 1 km for a given magnitude and stress, and $Y_{\mathrm{sim,1km}}(\mathbf{M},100\mathrm{bar})$ represents the ground motion simulated at D_{rup} = 1 km for the same magnitude, but for the reference stress (Δσ = 100 bar). Figure 4 shows the required stress adjustment factors as a function of Δσ, for various magnitudes and periods. This factor has an increasing trend with the stress, where $F_{\Delta\sigma}$ = 0 at Δσ = 100 bar, by definition. The slope of $F_{\Delta\sigma}$, which is defined by coefficient $e_{\Delta\sigma}$ in Equation 4, represents the strength of the ground-motion scaling with the stress parameter. The steeper the slope, the larger the influence of stress on ground motions. As seen in Figure 4, Δσ has significant influence at short periods (T < 0.2 s), regardless of

magnitude. However, its effects weaken with increasing period, particularly for small-to-moderate magnitude events (**M** < 6). For large magnitudes, the Δσ-effects extend to longer periods due to the shifting of the two corner frequencies with magnitude.

We regress the values of $e_{\Delta\sigma}$ (calculated for each magnitude and period from the values of $F_{\Delta\sigma}$ using Equation 4) to the functional form:

$$e_{\Delta\sigma} = \begin{cases} s_0 + s_1\mathbf{M} + s_2\mathbf{M}^2 + s_3\mathbf{M}^3 + s_4\mathbf{M}^4 & \Delta\sigma \leq 100 \text{ bar} \\ s_5 + s_6\mathbf{M} + s_7\mathbf{M}^2 + s_8\mathbf{M}^3 + s_9\mathbf{M}^4 & \Delta\sigma > 100 \text{ bar} \end{cases} \tag{17}$$

where s_0 to s_9 are period-dependent model coefficients. We use two polynomials, because we require a different shape for the $e_{\Delta\sigma}$ values for Δσ ≤ 100 bar and Δσ > 100 bar; we constrain the regressions to attain $F_{\Delta\sigma} = 0$ at Δσ = 100 bar. Figure 5 shows how the values of $e_{\Delta\sigma}$ vary with magnitude and period. The net effect of the stress parameter is complicated because of interactions between scaling of the high-frequency source amplitudes, shifting of the two corner frequencies, and changes in spectral sag between the corner frequencies. Additionally, the stress parameter affects the source duration, which in turn influences the response spectral amplitudes. Coupling of all these factors in the response spectrum domain requires a high-order polynomial to satisfactorily model Δσ-scaling over a wide period range. The values of model coefficients for the stress adjustment factor are listed in Table 3.

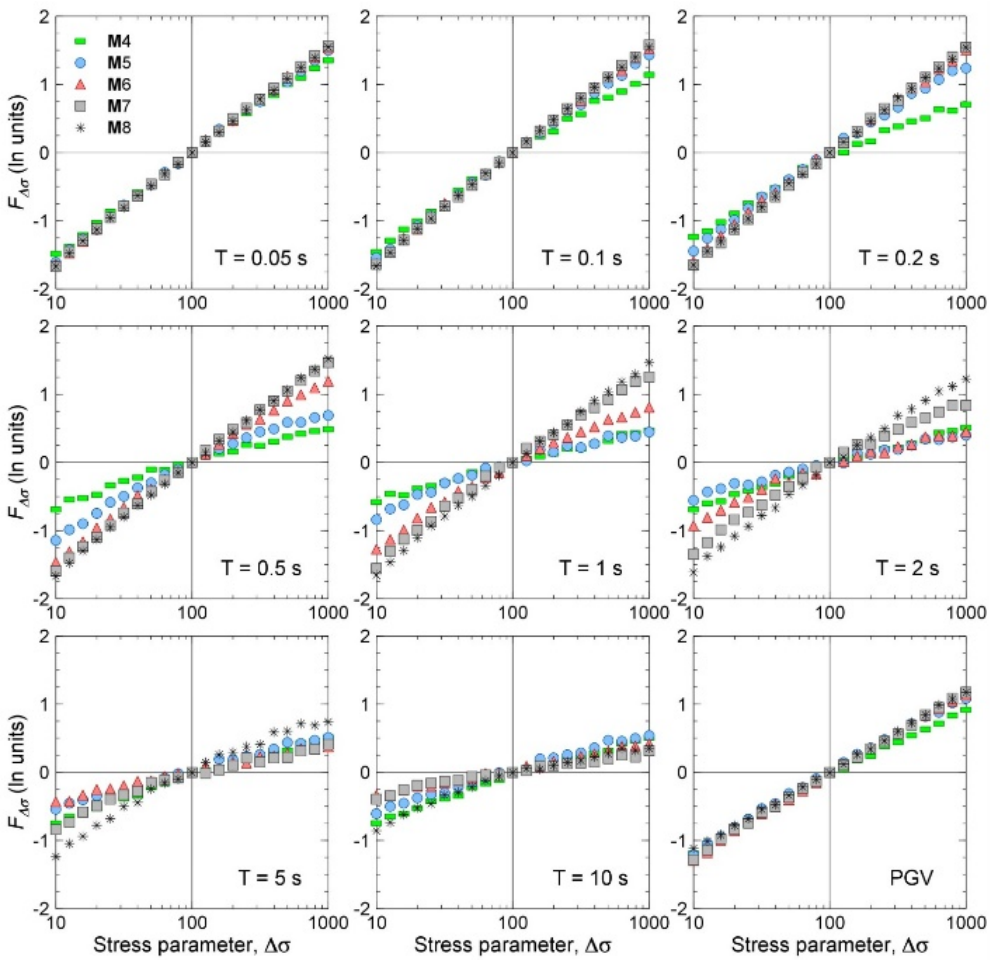

Figure 4. *Stress adjustment factors ($F_{\Delta\sigma}$) determined from simulations.*

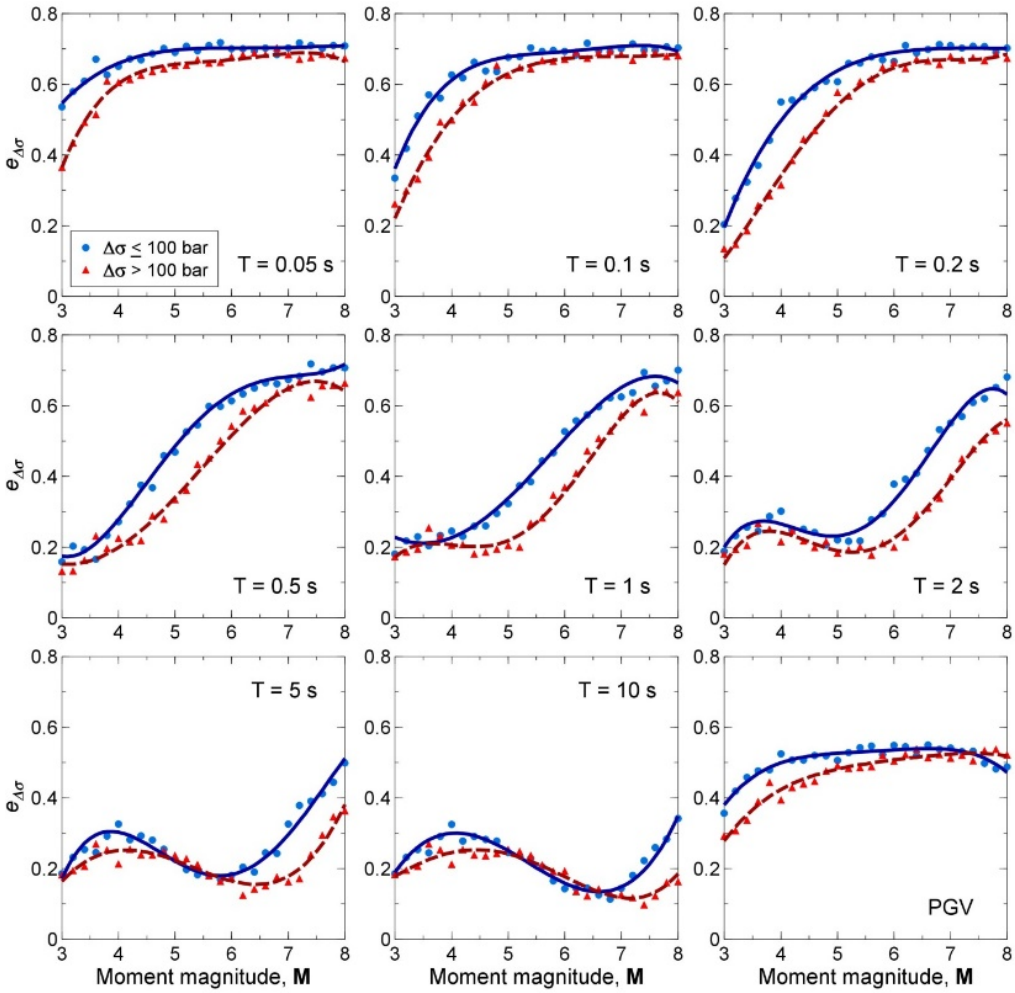

Figure 5. *Stress-scaling coefficients ($e_{\Delta\sigma}$) obtained from simulations (symbols) and the fitted model (Equation 17).*

Table 3. *Model coefficients of the stress adjustment factor ($F_{\Delta\sigma}$) in the generic GMPE*

T (s)	s_0	s_1	s_2	s_3	s_4
0.010	-2.05E+0	1.88E+0	-4.90E-1	5.67E-2	-2.43E-3
0.013	-1.92E+0	1.80E+0	-4.71E-1	5.47E-2	-2.36E-3
0.016	-1.71E+0	1.66E+0	-4.36E-1	5.09E-2	-2.20E-3
0.020	-1.16E+0	1.27E+0	-3.34E-1	3.91E-2	-1.70E-3
0.025	-1.54E+0	1.59E+0	-4.29E-1	5.10E-2	-2.24E-3
0.030	-1.06E+0	1.20E+0	-3.13E-1	3.62E-2	-1.55E-3
0.040	-8.57E-1	1.04E+0	-2.68E-1	3.08E-2	-1.33E-3
0.050	-9.63E-1	9.83E-1	-2.16E-1	2.08E-2	-7.42E-4
0.065	-2.23E+0	1.95E+0	-4.90E-1	5.49E-2	-2.29E-3
0.080	-3.68E+0	2.96E+0	-7.51E-1	8.42E-2	-3.51E-3
0.100	-4.05E+0	3.10E+0	-7.62E-1	8.33E-2	-3.39E-3
0.130	-4.17E+0	3.09E+0	-7.44E-1	7.98E-2	-3.21E-3

0.160	-3.96E+0	2.82E+0	-6.50E-1	6.72E-2	-2.61E-3
0.200	-2.71E+0	1.73E+0	-3.30E-1	2.82E-2	-9.06E-4
0.250	-1.77E+0	9.83E-1	-1.31E-1	6.00E-3	-1.16E-5
0.300	-3.18E-1	-1.39E-1	1.70E-1	-2.85E-2	1.42E-3
0.400	2.02E+0	-1.86E+0	6.12E-1	-7.67E-2	3.34E-3
0.500	3.96E+0	-3.29E+0	9.88E-1	-1.20E-1	5.14E-3
0.650	3.65E+0	-2.82E+0	7.93E-1	-8.93E-2	3.55E-3
0.800	2.40E+0	-1.65E+0	4.09E-1	-3.71E-2	1.05E-3
1.000	1.07E+0	-4.55E-1	3.74E-2	1.03E-2	-1.08E-3
1.300	-2.51E+0	2.52E+0	-8.45E-1	1.21E-1	-6.02E-3
1.600	-5.26E+0	4.74E+0	-1.48E+0	1.96E-1	-9.28E-3
2.000	-6.64E+0	5.77E+0	-1.74E+0	2.24E-1	-1.03E-2
2.500	-8.08E+0	6.84E+0	-2.02E+0	2.54E-1	-1.14E-2
3.000	-7.98E+0	6.64E+0	-1.92E+0	2.37E-1	-1.04E-2
4.000	-7.12E+0	5.78E+0	-1.61E+0	1.90E-1	-7.98E-3
5.000	-6.39E+0	5.08E+0	-1.38E+0	1.58E-1	-6.36E-3
6.500	-4.80E+0	3.68E+0	-9.37E-1	9.76E-2	-3.47E-3
8.000	-3.42E+0	2.51E+0	-5.80E-1	5.15E-2	-1.34E-3
10.000	-2.19E+0	1.51E+0	-2.87E-1	1.53E-2	2.38E-4
PGA	-2.13E+0	1.94E+0	-5.04E-1	5.82E-2	-2.50E-3
PGV	-2.25E+0	1.95E+0	-5.18E-1	6.14E-2	-2.73E-3

Table 3. *(cont'd)*

T (s)	s_5	s_6	s_7	s_8	s_9
0.010	-1.44E+0	1.24E+0	-2.89E-1	3.09E-2	-1.25E-3
0.013	-1.35E+0	1.20E+0	-2.80E-1	3.01E-2	-1.23E-3
0.016	-1.08E+0	1.04E+0	-2.47E-1	2.69E-2	-1.11E-3
0.020	-1.27E+0	1.25E+0	-3.17E-1	3.62E-2	-1.55E-3
0.025	-1.45E+0	1.37E+0	-3.37E-1	3.73E-2	-1.54E-3
0.030	-2.24E+0	1.98E+0	-5.09E-1	5.78E-2	-2.44E-3
0.040	-3.31E+0	2.66E+0	-6.68E-1	7.42E-2	-3.06E-3
0.050	-4.23E+0	3.29E+0	-8.32E-1	9.30E-2	-3.87E-3
0.065	-3.96E+0	2.87E+0	-6.67E-1	6.88E-2	-2.65E-3
0.080	-3.14E+0	2.18E+0	-4.67E-1	4.47E-2	-1.60E-3
0.100	-2.45E+0	1.57E+0	-2.89E-1	2.30E-2	-6.57E-4
0.130	-1.38E+0	6.26E-1	-1.16E-2	-1.09E-2	8.28E-4
0.160	-2.00E-1	-3.37E-1	2.57E-1	-4.25E-2	2.18E-3
0.200	8.20E-1	-1.08E+0	4.40E-1	-6.10E-2	2.85E-3
0.250	1.78E+0	-1.77E+0	6.07E-1	-7.83E-2	3.50E-3
0.300	2.25E+0	-2.00E+0	6.33E-1	-7.70E-2	3.27E-3

0.400	2.42E+0	-1.94E+0	5.56E-1	-6.17E-2	2.39E-3
0.500	8.56E-1	-4.53E-1	6.46E-2	5.22E-3	-8.30E-4
0.650	-6.67E-1	9.28E-1	-3.71E-1	6.18E-2	-3.43E-3
0.800	-2.12E+0	2.15E+0	-7.30E-1	1.05E-1	-5.29E-3
1.000	-4.47E+0	4.05E+0	-1.27E+0	1.71E-1	-8.14E-3
1.300	-5.49E+0	4.77E+0	-1.44E+0	1.85E-1	-8.46E-3
1.600	-5.88E+0	4.98E+0	-1.46E+0	1.83E-1	-8.16E-3
2.000	-6.01E+0	4.99E+0	-1.43E+0	1.75E-1	-7.59E-3
2.500	-4.88E+0	3.95E+0	-1.09E+0	1.26E-1	-5.17E-3
3.000	-4.18E+0	3.32E+0	-8.86E-1	9.89E-2	-3.85E-3
4.000	-2.63E+0	1.96E+0	-4.62E-1	4.24E-2	-1.18E-3
5.000	-1.38E+0	9.09E-1	-1.42E-1	1.32E-3	7.11E-4
6.500	-3.93E-1	9.83E-2	9.53E-2	-2.78E-2	1.96E-3
8.000	-6.87E-3	-1.89E-1	1.69E-1	-3.53E-2	2.20E-3
10.000	2.68E-1	-3.86E-1	2.17E-1	-3.97E-2	2.30E-3
PGA	-1.44E+0	1.24E+0	-2.85E-1	3.02E-2	-1.22E-3
PGV	-1.76E+0	1.38E+0	-3.26E-1	3.50E-2	-1.42E-3

Adjustment of the generic model to a specific region includes any required modifications to the source and attenuation parameters, as well as determination of an empirical calibration factor that accounts for residual effects that are missing and/or different in the simulations compared to the observed motions. In this study, we assume that the magnitude (F_M) and saturation (h) effects determined from simulations are transferable to other regions. However, the stress parameter may vary regionally; the generic GMPE is directly adjusted for this effect when the regional value of stress parameter is plugged into $F_{\Delta\sigma}$. The required modifications for regional attenuation can be done by means of Z and γ. We recommend keeping the presumed Z model (geometric spreading) as it is defined in the generic model, unless there is compelling evidence for its modification. The anelastic attenuation coefficient, γ, is determined using empirical data at regional distances for the region of interest; such data can be obtained from weak-motion studies. The calibration factor, C, is calculated through the analysis of residuals between observed motions in the target region and the GMPE, after application of the regional values of $\Delta\sigma$, Z and γ. Table 4 provides the values of the calibration and anelastic terms for California that match the simulations to the model described by Yenier and Atkinson (2014b), as determined using the methodology described in the next section. This enables comparisons of the California model with the adjusted model for CENA, which we now describe.

Table 4. *Anelastic attenuation and calibration coefficients to adjust the generic GMPE for CENA. The corresponding values for California are also shown.*

T (s)	$\gamma_{California}$	$C_{e,California}$	γ_{CENA}	$C_{e,CENA}$	$\Delta b_{3\ (CENA)}$
0.010	-1.44E-2	2.41E-2	-4.66E-3	-3.98E-2	3.81E-2
0.013	-1.45E-2	2.99E-2	-4.69E-3	-3.86E-2	3.45E-2
0.016	-1.44E-2	1.77E-2	-4.69E-3	-8.94E-2	3.35E-2
0.020	-1.44E-2	-1.20E-2	-4.67E-3	-1.82E-1	3.51E-2
0.025	-1.51E-2	-5.99E-2	-4.88E-3	-2.09E-1	1.97E-2

0.030	-1.58E-2	-9.15E-2	-5.11E-3	-2.64E-1	1.74E-2
0.040	-1.62E-2	-1.07E-1	-5.27E-3	-4.59E-1	1.18E-2
0.050	-1.69E-2	-9.20E-2	-5.47E-3	-4.91E-1	2.07E-2
0.065	-1.76E-2	-5.97E-2	-5.71E-3	-2.99E-1	2.49E-2
0.080	-1.79E-2	-4.59E-2	-5.79E-3	-1.95E-1	4.82E-2
0.100	-1.74E-2	2.41E-2	-5.64E-3	-1.72E-1	7.27E-2
0.130	-1.61E-2	2.99E-2	-5.24E-3	-5.85E-2	9.53E-2
0.160	-1.47E-2	1.77E-2	-4.77E-3	-7.95E-2	9.84E-2
0.200	-1.30E-2	-1.20E-2	-4.20E-3	-1.05E-1	1.15E-1
0.250	-1.12E-2	-5.99E-2	-3.65E-3	-1.69E-1	1.16E-1
0.300	-9.62E-3	-9.15E-2	-3.12E-3	-2.48E-1	1.20E-1
0.400	-7.51E-3	-1.07E-1	-2.44E-3	-3.34E-1	8.92E-2
0.500	-6.29E-3	-9.20E-2	-2.04E-3	-3.66E-1	8.08E-2
0.650	-5.05E-3	-5.97E-2	-1.64E-3	-3.88E-1	6.09E-2
0.800	-4.40E-3	-4.59E-2	-1.43E-3	-3.85E-1	6.55E-2
1.000	-3.88E-3	-5.93E-3	-1.26E-3	-3.73E-1	7.37E-2
1.300	-3.28E-3	3.66E-2	-1.06E-3	-3.70E-1	9.31E-2
1.600	-3.61E-3	5.19E-2	-1.17E-3	-3.03E-1	1.17E-1
2.000	-3.13E-3	8.44E-2	-1.02E-3	-3.01E-1	1.11E-1
2.500	-3.27E-3	1.42E-1	-1.06E-3	-2.09E-1	8.87E-2
3.000	-2.83E-3	2.19E-1	-1.09E-3	-6.05E-2	9.73E-2
4.000	-2.12E-3	3.04E-1	-1.30E-3	5.03E-2	1.00E-1
5.000	-1.70E-3	4.36E-1	-9.35E-4	1.75E-2	1.00E-1
6.500	-1.31E-3	5.49E-1	-7.87E-4	4.18E-1	1.00E-1
8.000	-1.06E-3	6.29E-1	-6.43E-4	1.66E-1	1.00E-1
10.000	-8.49E-4	7.17E-1	-3.65E-4	3.72E-1	1.00E-1
PGA	-1.44E-2	2.41E-2	-4.67E-3	-1.96E-2	3.78E-2
PGV	-8.61E-3	8.44E-2	-2.79E-3	-2.10E-1	5.18E-2

An Example Application: Adjustment of the Generic GMPE for CENA

As an example implementation of the method, we adjust the generic GMPE for the central and eastern North America (CENA) using ground motions obtained in the region. We use the database of PGA, PGV and 5%-damped PSA from the NGA-East flatfile (see Data and Resources), for CENA earthquakes of $\mathbf{M} \geq 3.0$ that were recorded by at least three stations within 600 km. We consider both natural and induced earthquakes in the region. However, ground motions recorded in the Gulf Coast regions are excluded due to considerably different attenuation attributes in this region (EPRI, 2004). We use the average orientation-independent horizontal-component ground motions calculated based on the RotD50 measure (Boore, 2010), as provided in NGA-East flatfile; this is approximately equivalent to geometric mean motions as provided in the simulations. Figure 6 shows a map of the epicenters of the study events and Figure 7 is a map of stations and their site condition. Figure 8 shows the magnitude-distance distribution of the selected records.

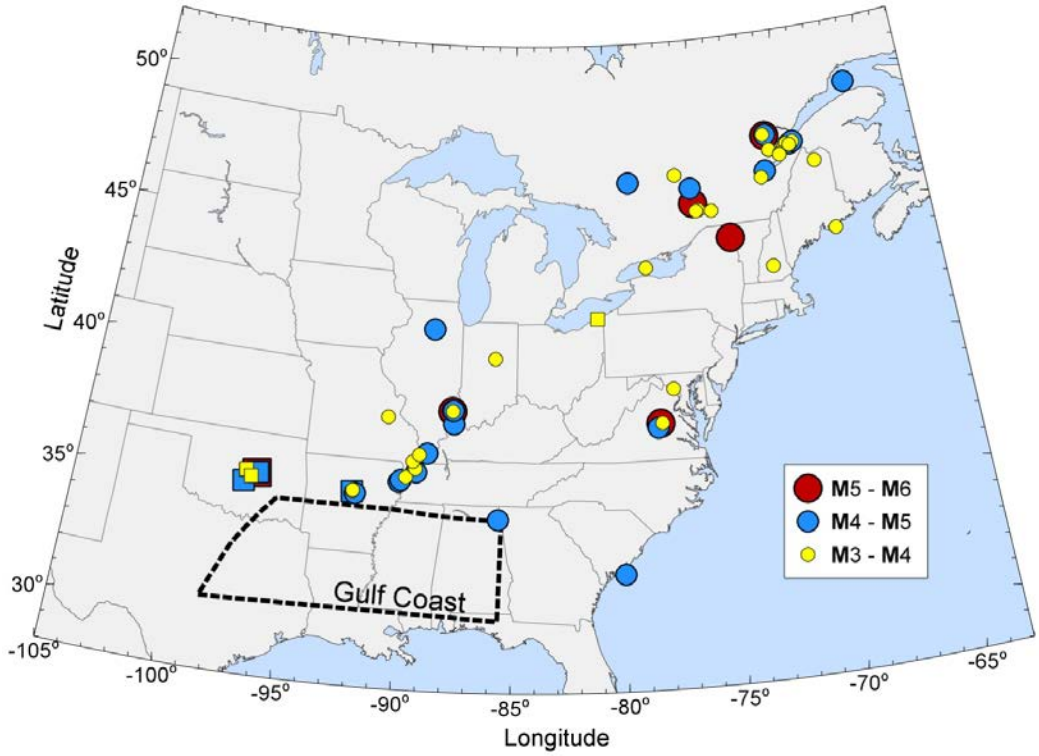

Figure 6. *Epicenters of study events in central and eastern North America (CENA). Circles show epicenter locations of naturally-occurring earthquakes and squares indicate events that have been flagged as potentially induced in the NGA-East flatfile. Dashed line marks the Gulf Coast region.*

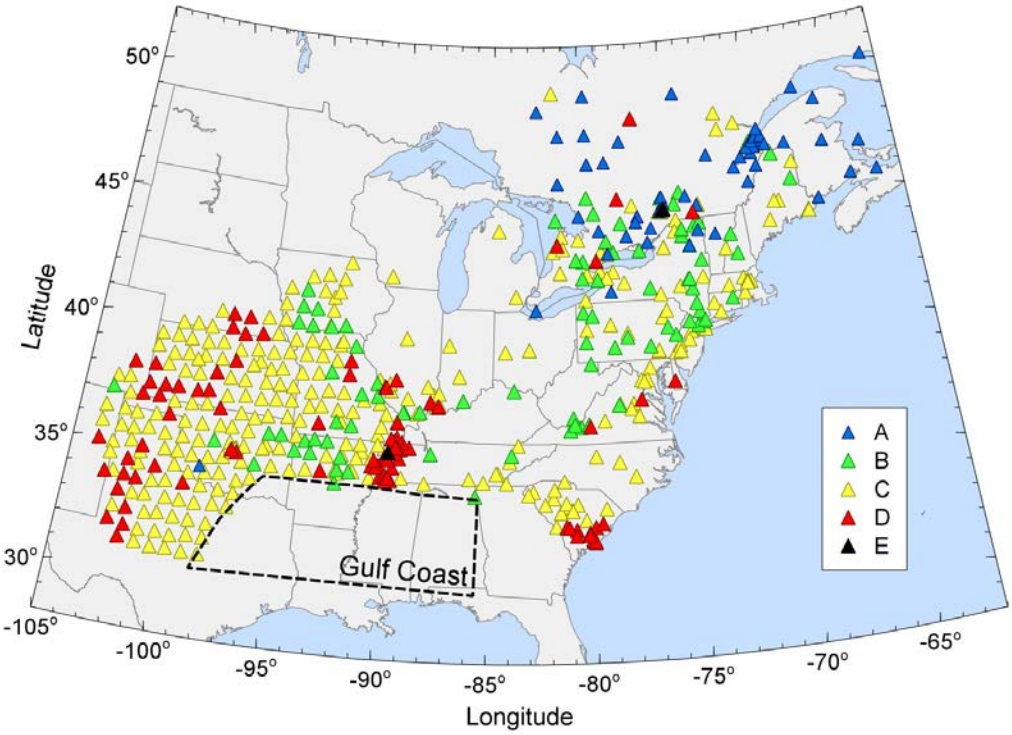

Figure 7. *Locations of recording stations and their NEHRP (National Earthquake Hazards Reduction Program) site classification: A: VS30 > 1500 m/s, B: 760 m/s < VS30 ≤ 1500 m/s, C: 360 m/s < VS30 ≤ 760 m/s, D: 180 m/s < VS30 ≤ 360 m/s and E: VS30 ≤ 180 m/s (NEHRP, 2000). We excluded stations located in the Gulf Coast region (dashed line).*

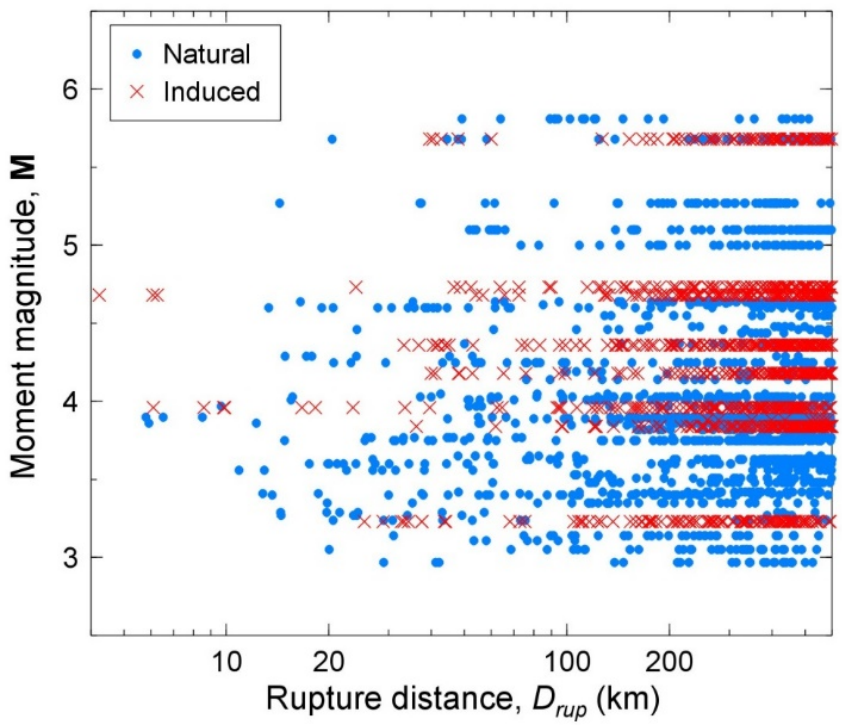

Figure 8. *Magnitude-distance distribution of the selected ground motions in CENA. Ground motions recorded beyond 600 km are not considered.*

In the analysis, we consider response spectra up to a maximum usable period to reduce the impact of long-period noise on the adjusted GMPE. For a given ground-motion record, the maximum usable period, T_{max}, is defined as

$$T_{max} = \frac{1}{\max[(1.25 f_{lc}), (f_{min})]} \tag{18}$$

where f_{lc} is the low-cut filter frequency of the record reported in the NGA-East flatfile and f_{min} is the limiting frequency below which spectral amplitudes are assumed to be noise-dominated. We describe f_{min} as

$$f_{min} = max\left[(0.1), \left(10^{\,0.75-\mathbf{M}/3}\right)\right] \tag{19}$$

Equation 19 is defined such that it provides an overall agreement with the geometric mean of the factored filter frequencies (i.e., $1.25f_{lc}$), as seen in Figure 9. For $\mathbf{M} < 6$, the f_{min} model given for CENA is relatively less conservative than that was used for California by Yenier and Atkinson (2014b) because ground motions attenuate more slowly in CENA, providing useable signal to greater distances.

We correct the recorded ground-motion amplitudes to the equivalent values for NEHRP B/C site conditions (V_{S30} = 760 m/s) using the F_S function adopted from BSSA14. This function is based on the values of V_{S30} and PGA_r for each record, where the V_{S30} values are given in the NGA-East flatfile, and we assume that PGA_r can be reasonably estimated from BSSA14 as an approximation. We deliberately use BSSA14 rather than a CENA GMPE for this purpose, as we do not wish the higher frequency content in CENA to impose greater nonlinearity.

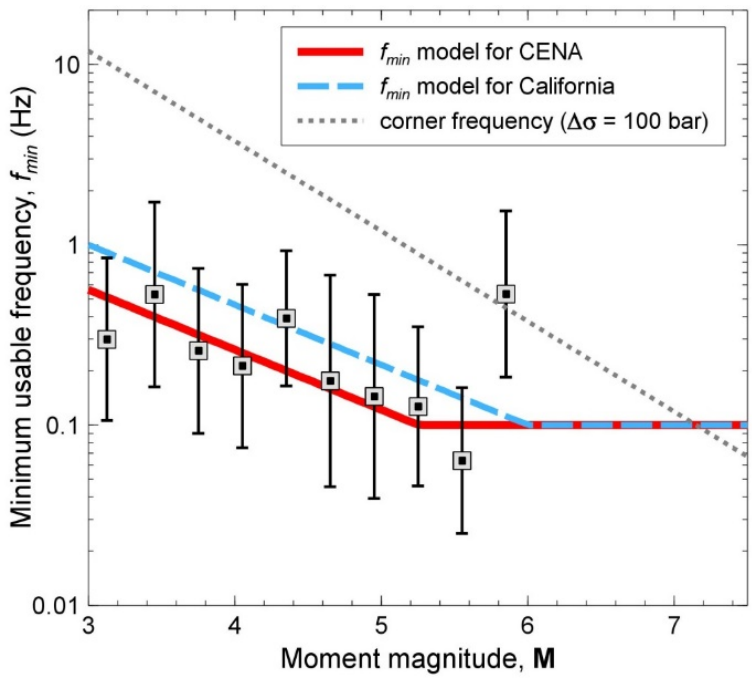

Figure 9. *Minimum usable frequency (f_{min}) model considered for records in CENA (solid line). Squares indicate the geometric mean of the factored low-cut filter frequencies (i.e., $1.25f_{lc}$) determined for evenly-spaced magnitude bins. The error bars represent one standard deviation about the mean values. The dashed line indicates the f_{min} model used for California by Yenier and Atkinson (2014b). The dotted line shows the corner frequency of the Brune (1970) source model for $\Delta\sigma$ = 100 bar.*

<u>*Regional Attenuation*</u>

Empirical studies suggest that the geometrical spreading of Fourier amplitudes in CENA can be adequately described as $R^{-1.3}$ within 50 km and $R^{-0.5}$ at further distances (Atkinson and Boore, 2014; Babaie Mahani and Atkinson, 2012). We therefore use the generic bilinear Z model (b_1 = -1.3, b_2 = -0.5 and R_t = 50 km) without modification. The only attenuation adjustment needed is for the regional anelastic attenuation. As described in the methodology presented earlier, we determine the regional anelastic attenuation (γ_{CENA}) from the empirical data using:

$$\ln Y_{B/C,ij} - \left(F_{M,i} + F_{Z,ij}\right) = E_i + \gamma_{CENA} D_{rup,ij} \tag{20}$$

where $Y_{B/C,ij}$ represents the B/C-corrected motion for event i and station j. $F_{M,i}$ and $F_{Z,ij}$ are the magnitude and geometrical spreading functions evaluated for the known magnitude and distance ($D_{rup,ij}$) of the record, respectively. The E_i term is an event term, which provides the average adjustment required to match observed amplitudes from event i. Its value can be attributed to two main factors: (i) the difference between the reference stress implicitly carried by the F_M function (100 bars) and its true value for the ith event (modeled by $F_{\Delta\sigma}$), and (ii) the overall difference between synthetics and observed motions in CENA (modeled by C). We calculate the regional anelastic attenuation coefficient (γ_{CENA}) and event terms (E_i) for each oscillator period and ground motion parameter; the values of the γ_{CENA} term are listed Table 4.

<u>*Regional Stress Parameter*</u>

The stress parameter is often determined by matching the predicted and observed spectral amplitudes at short periods for the specified moment. However, this approach results in a non-unique solution for Δσ due to the

trade-off between earthquake source and attenuation (Boore et al., 2010; Yenier and Atkinson, 2014a). Moreover, Δσ has little effect on the response spectrum at long periods (Figures 4), especially for small-to-moderate events, restricting our ability to calibrate the response spectral amplitudes at long periods. To ensure a model calibration that is consistent over a wide period range, we determine the stress parameter by matching the observed spectral shape for the known moment (i.e. the corner frequency), rather than spectral amplitudes. This breaks the trade-off between source and attenuation parameters, transferring the overall amplitude difference to the calibration factor *C* (Yenier and Atkinson, 2014b). Following this technique, we use a grid search to determine Δσ for each event separately. We select the best-fitting Δσ based on the minimum standard deviation of residuals between E_i and $F_{\Delta\sigma}$, over a wide period range (0.01 s ≤ T ≤ 10 s); by minimizing the standard deviation of residuals, we are effectively finding the best shape, rather than the best level.

Figure 10 shows the shape-based Δσ values obtained from CENA events as a function of focal depth (*d*). The mean stress determined for evenly-spaced focal depth bins shows an increasing trend from Δσ ≈ 30 bar at *d* = 2.5 km to Δσ ≈ 250 bar at *d* = 10 km; it remains relatively constant at greater depths. Figure 11 shows the best-fitting Δσ as a function of magnitude. For **M** < 5, the stress parameter shows large variability. Despite the large variation of Δσ values at small magnitudes, the depth effect is clearly visible by the distinct separation of depth-clustered stresses. For **M** > 5, the stress parameter attains a value of Δσ ≈ 300 bars, on average; we note that this is about three times the corresponding value of 100 bars for California events.

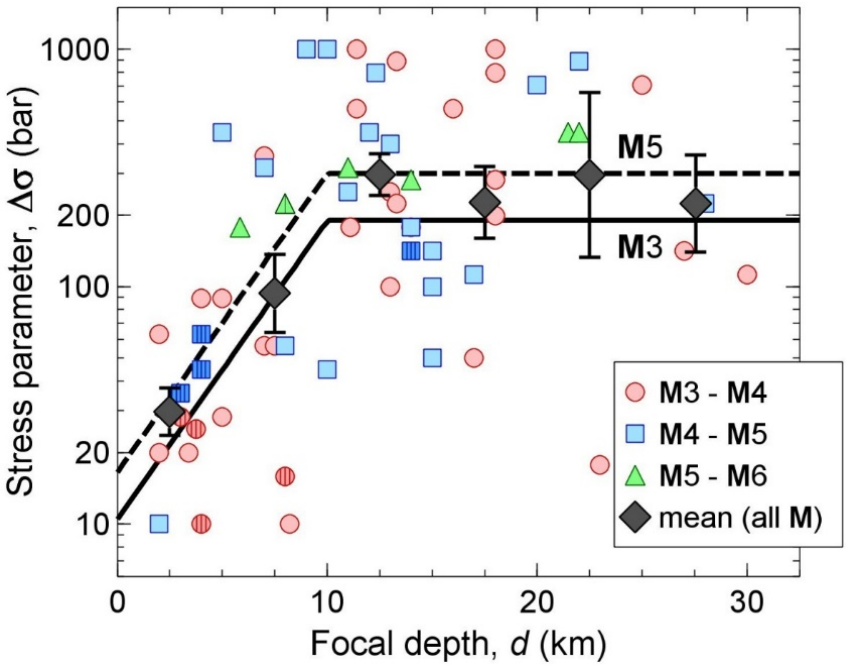

Figure 10. *Best-fitting stress parameters (Δσ) determined for CENA events as a function of focal depth (d). Δσ values are clustered into different magnitude bins as shown in the legend. Hatched symbols indicate Δσ values obtained from the induced events. Diamonds represent the mean Δσ calculated for evenly-spaced focal depth bins over all magnitudes, and the error bars show standard error about the mean stress. Lines indicate the derived Δσ model (Equation 21) evaluated for* ***M****3 (solid) and* ***M****5 (dashed).*

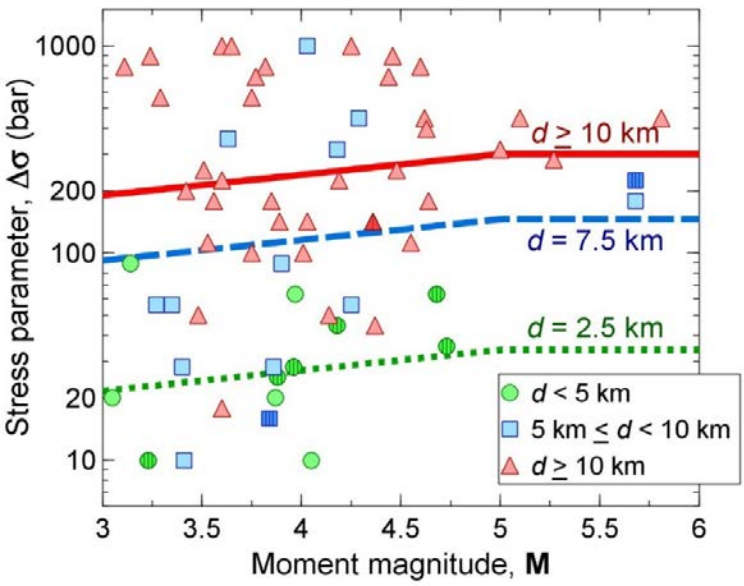

Figure 11. *Best-fitting stress parameters (Δσ) determined based on matching the observed response spectral shape for CENA events, as a function of magnitude. Δσ values are clustered into different focal depth (d) bins as shown in the legend. Hatched symbols show Δσ values obtained from the induced events. Lines indicate the derived Δσ model (Equation 21) evaluated for d = 2.5 km (dotted) d = 7.5 km (dashed) and d ≥ 10 km (solid).*

We regress the best-fitting Δσ values to develop a regional stress model for CENA. Based on the observations made in Figures 10 and 11, we constrain the model to attain Δσ = 300 bar for **M** ≥ 5 and *d* ≥ 10 km. The mean value of the stress parameter for earthquakes in CENA is expressed as:

$$\ln\Delta\sigma_{CENA} = 5.704 + \min[0,\ \ 0.29(d-10)] + \min[0,\ \ 0.229(\mathbf{M}-5)] \qquad (21)$$

The estimates of Equation 21 for different magnitudes and depths are shown in Figures 10 and 11. The mean residuals between the observed and predicted Δσ values attain values around zero, as illustrated in Figure 12. Overall, the proposed Δσ model provides a good agreement with the Δσ values determined from CENA events based on the inferred spectral shape.

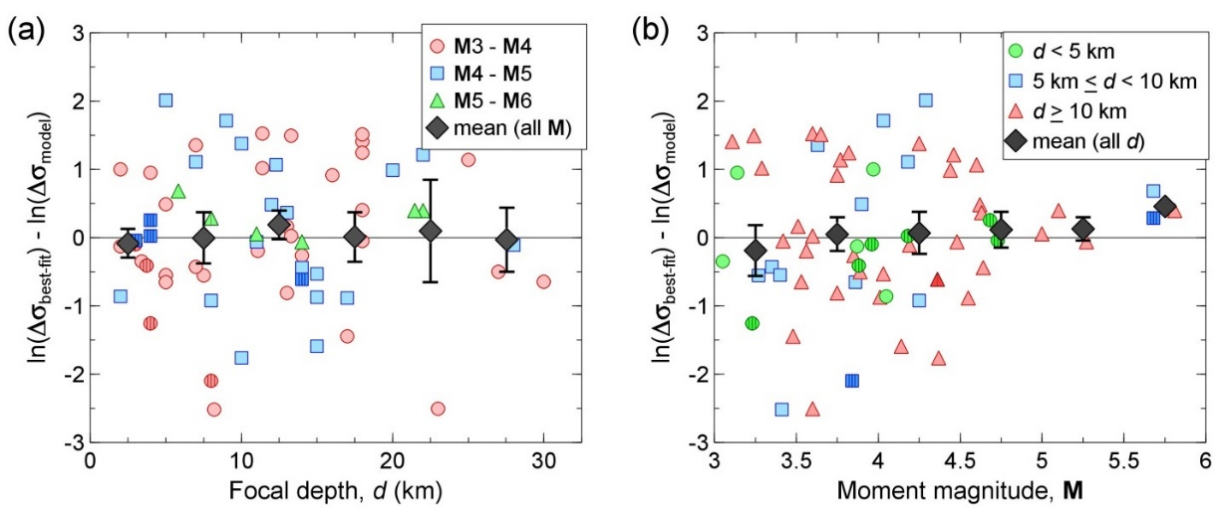

Figure 12. *Residuals between the best-fitting Δσ values obtained from CENA events and the estimates of the Δσ model (Equation 21) evaluated for the known magnitudes and focal depths of the study events.*

Calibration Factor

An overall calibration factor is needed to reconcile the predictions with observed amplitudes in the target region, accounting for effects missing and/or different in simulations (e.g., discrepancies between the assumed and true values of crustal properties, site amplification, κ_0 and path duration). We calculate the calibration factor based on the analysis of residuals:

$$\delta_{ij} = \ln Y_{B/C,ij} - \left(F_{M,i} + F_{\Delta\sigma CENA,i} + F_{Z,ij} + \gamma_{CENA} D_{rup,ij}\right) \quad (22)$$

where δ_{ij} represents the residual for the ground motion obtained from event i at station j, for a given spectral period or peak motion. $F_{\Delta\sigma CENA,i}$ is the stress adjustment factor evaluated for $\Delta\sigma$ from Equation 21 for the known magnitude and focal depth of event i. The last term accounts for the regional anelastic attenuation determined earlier.

Figure 13 shows the event residuals ($\delta_i = \sum\delta_{ij}/n_i$, where n_i is the number of records obtained from event i; $n_i \geq 3$ at a given period) as a function of magnitude. δ_i generally attains negative values and appears to be randomly distributed, showing no distinct attributes for natural and induced events. The mean δ_i values determined at evenly-spaced magnitude bins shows no magnitude-dependent trends, in general. This suggests that the magnitude scaling of ground motions in CENA is well captured by the F_M function, at least for the available data. Based on these observations, we calculate an event-based calibration factor (C_e) as the average of δ_i values over all magnitudes, for each spectral period/peak motion, as listed in Table 4. The C_e term fluctuates with period between 0 and -0.5 (ln units) for periods T < 3 s and attains positive values with an increasing trend at larger periods, as shown in Figure 14. This increasing trend at long periods may be due to the fact that stochastic simulations are inherently limited in their ability to generate the coherent motions seen at long periods.

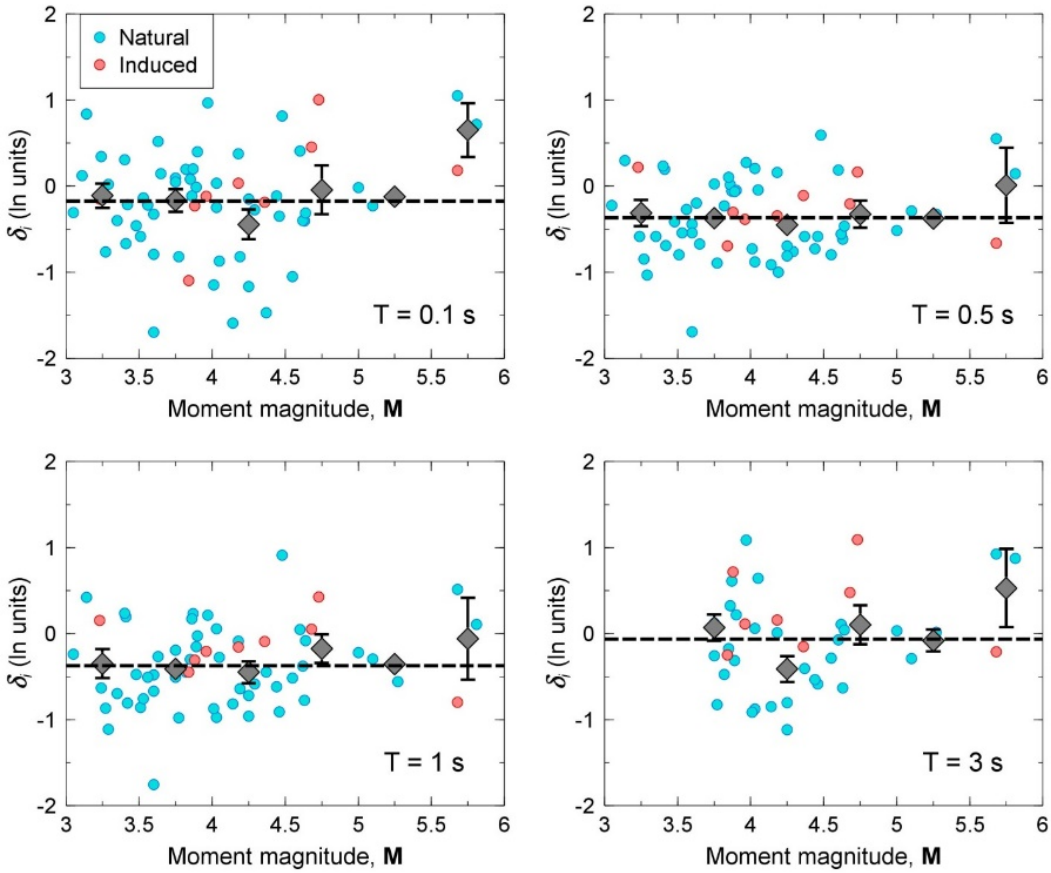

Figure 13. *Average of residuals determined for each event that have at least 3 observations at a given period (δ_i, circles). Diamonds show mean of δ_i values determined for evenly-spaced magnitude bins, and error bars represent the standard error about the mean. Dashed lines indicate the event-based calibration factors (C_e) that is defined as the average of δ_i values over all magnitudes, at a given period.*

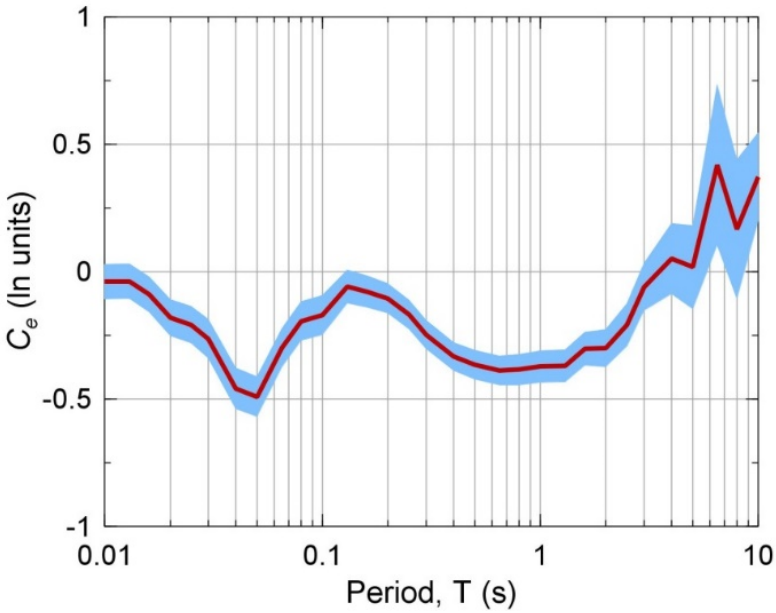

Figure 14. *Event-based calibration factor (C_e, solid line) for CENA events. Shaded area represents the standard error about C_e.*

We subtract the event-based δ_i term from the individual residuals to calculate the average residual at each station (i.e., $\delta_j = \sum(\delta_{ij} - \delta_i)/n_j$, where n_j is the number of observations at station j; $n_j \geq 3$ at a given period). Figure 15 illustrates the variation of δ_j as a function of V_{S30}. The mean δ_j determined at NEHRP B and C sites attain values near zero, in general, suggesting that the BSSA14 site amplification model is reasonable for these sites. However, ground motions on NEHRP A sites are underpredicted by ~15% and ground motions at NEHRP D sites are overpredicted by ~20%, on average. This might be related to the uneven spatial distribution of NEHRP A and D stations in the region, as shown in Figure 7. Anelastic attenuation to the north (Canadian sites) might be slightly lower than the average anelastic attenuation determined from the entire region. This may result in underprediction of observed motions for the Canadian stations, which are mostly on NEHRP A sites. Similarly, low Q characteristics nearer to the Gulf Coast may lead to overprediction of ground motions in the Mississippi region, which are mostly located on NEHRP D sites.

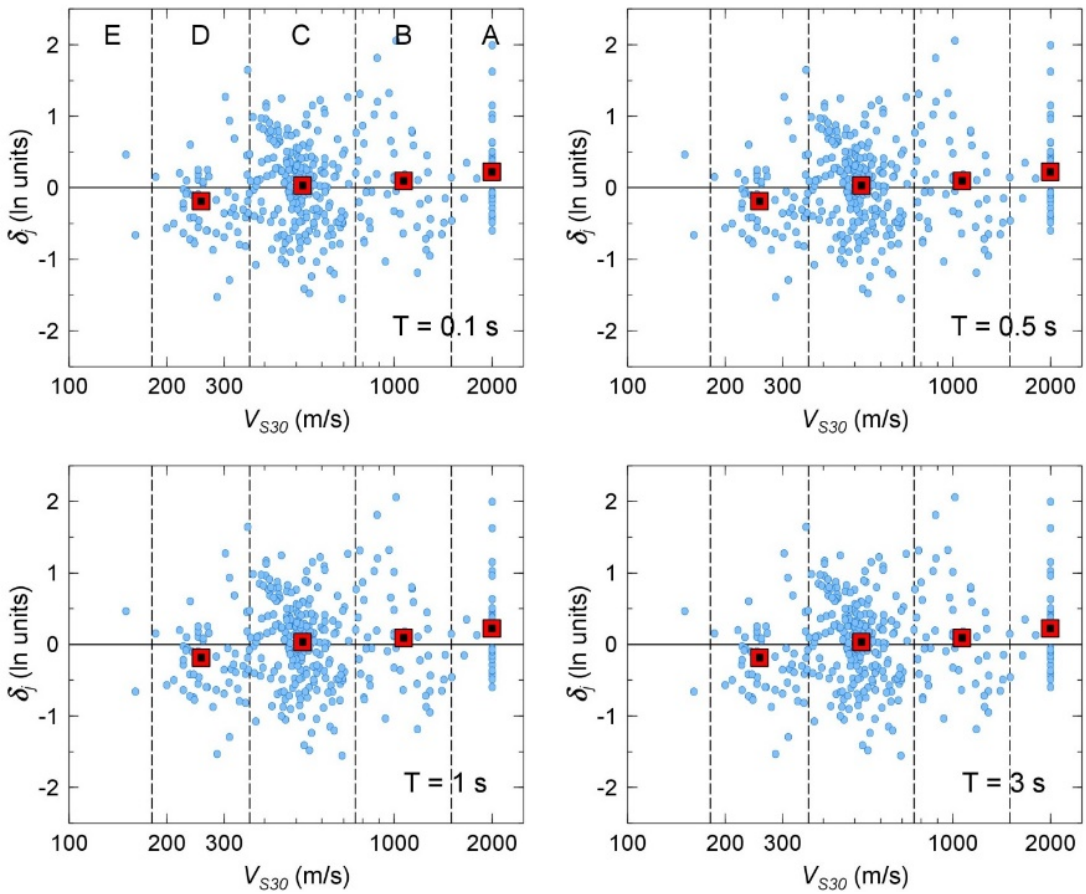

Figure 15. *Event-corrected average residuals for each station (δ_j, circles) as a function of V_{S30}. Mean of δ_j values for NEHRP site classes are shown by squares (standard errors for the mean values are smaller than the symbols).*

Finally, we correct the individual residuals for the event and station terms (i.e., $\delta'_{ij} = \delta_{ij} - \delta_i - \delta_j$) to assess the performance of the assumed geometrical spreading function. Figure 16 compares the δ'_{ij} values as a function of rupture distance. The mean δ'_{ij} determined for log-spaced distance bins attains near zero values at $D_{rup} > 150$ km, suggesting that γ_{CENA} parameter can successfully represent the overall attenuation at far distances. However, the mean δ'_{ij} deviates from the horizontal zero-line and decreases with distance for $D_{rup} < 150$ km, as shown in the figure. This discrepancy might be attributable to the path-duration model. In the simulations, we used a

path-duration model derived primarily from observed motions in WNA. Boore and Thompson (2015) recently reported that the path duration in ENA is much longer than that in WNA, particularly at distances less than 150 km. This difference could result in some overestimation of CENA motions for D_{rup} < 150 km because the presumed WNA path-duration model is implicitly carried via the F_Z function to CENA.

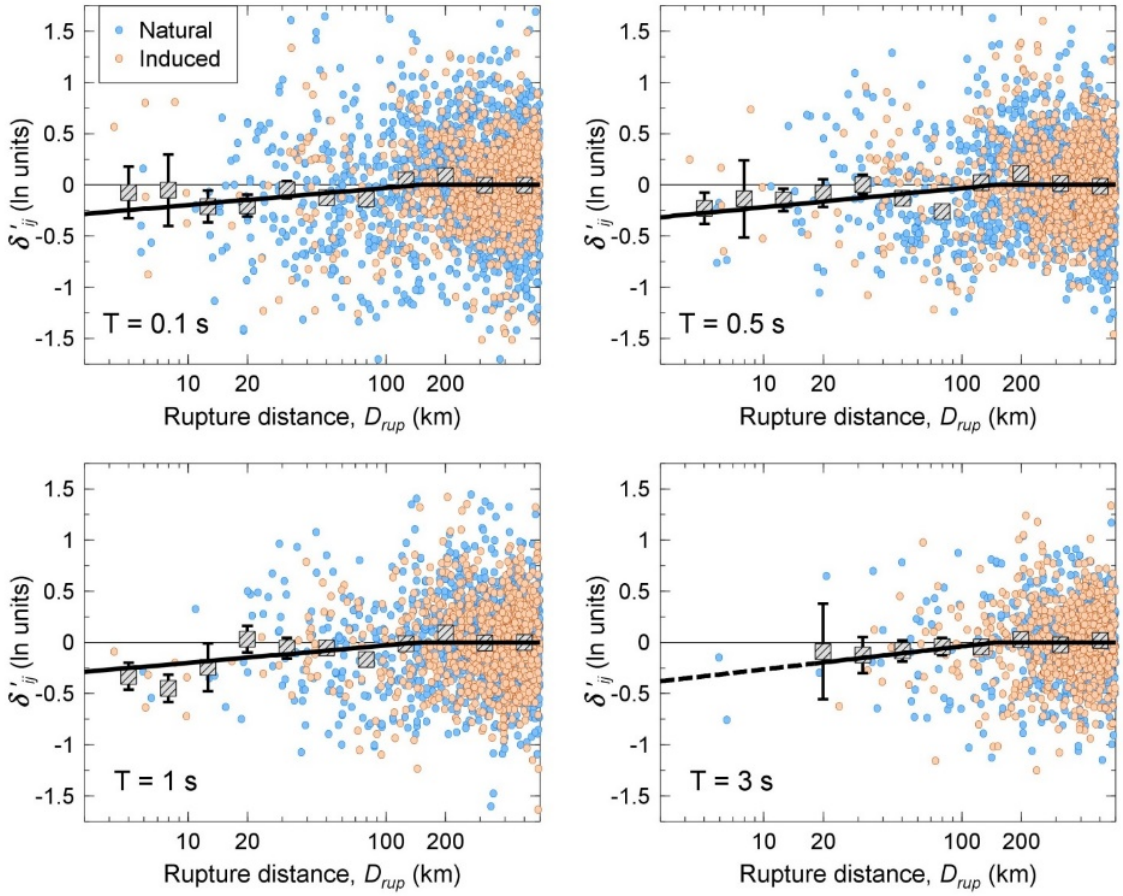

Figure 16. *Event- and site-corrected residuals (δ'_{ij}) as a function of distance, for ground motions obtained from natural and induced events. Squares show the mean δ'_{ij} values determined for logarithmically-spaced distance bins and error bars indicate the standard error about the mean. Solid line represents the fitted path-related calibration model (C_p).*

We consider an additional minor calibration term for regional differences in the path duration. We describe this path-related calibration (C_p) as:

$$C_p = \begin{cases} \Delta b_3 \ln(R/150) & R \leq 150\ km \\ 0 & R > 150\ km \end{cases} \tag{23}$$

where Δb_3 represents a calibration for the geometrical attenuation rate in response spectrum domain. We determine the Δb_3 term from the regression of δ'_{ij} based on Equation 23 at each period and peak motion separately. Its value could be determined only up to T = 3 s due to the limited data at D_{rup} < 100 km for longer periods. For periods T > 3 s, we recommend an average value of Δb_3 = 0.1 obtained from T > 1 s. Table 4 lists the values of Δb_3 for all periods and peak motions.

The total calibration needed for the adjusted GMPE is the summation of C_e and C_p terms. This closes the systematic gaps between simulation-based predictions and observed motions in CENA. The resultant CENA-adjusted prediction equation is given as:

$$\ln Y_{CENA} = F_M + F_{\Delta\sigma CENA} + F_Z + \gamma_{CENA} D_{rup} + F_S + C_e + C_p \tag{24}$$

Figure 17 illustrates PSA values predicted from Equation 24 for magnitudes **M**4 to **M**8 as a function of rupture distance, for NEHRP B/C site condition (V_{S30} = 760 m/s). The B/C-corrected ground motions obtained from earthquakes in CENA are also shown in the figure, for two magnitude ranges: **M**3.5-**M**4.5 and **M**4.5-**M**5.5. The CENA-adjusted GMPE is in good agreement with the empirical data, where available, and provides seismologically-informed predictions of average ground motions for moderate-to-large magnitudes (**M** > 6).

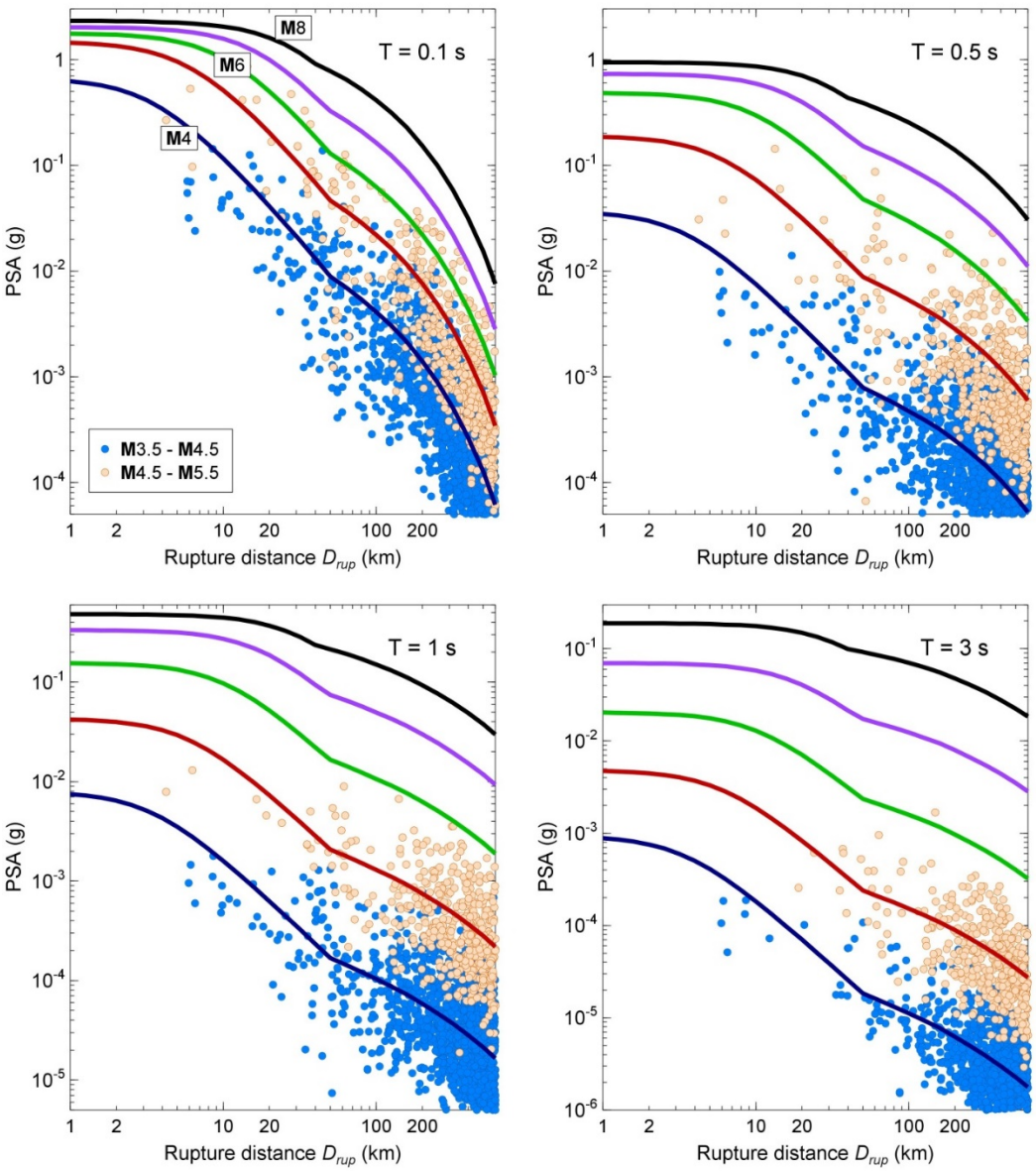

Figure 17. *PSA predictions from the adjusted GMPE (Equation 24) for magnitudes **M**4 to **M**8, for V_{S30} = 760 m /s (lines). Circles represent the B/C-corrected ground motions obtained from earthquakes in CENA for two magnitude ranges: **M**3.5-**M**4.5 and **M**4.5-**M**5.5.*

We conclude that the generic GMPE approach provides a calibrated model of predicted ground motions in CENA that agrees with average motions from the NGA-East database, and is constrained by simulation-based scaling principles that have been demonstrated to work in California over a wide range of magnitudes and distances. We have provided calibrated median predictions of ground motions in CENA for average horizontal-component peak ground motions and 5%-damped response spectra (up to T = 10 s), for magnitudes **M**3 to **M**8 and distances < 600 km. The approach that we have taken, in casting our model into a framework that is parameterized by the basic seismological parameters of moment, stress, and attenuation, has both conceptual and practical advantages. We can easily create understandable and documentable alternative GMPEs, by considering a range of possible parameter values that might be reasonable for the region (or a subset of the region). For each parameter set, we may use the empirical data to derive a new calibration factor for each frequency, such that the overall residuals are minimized for the given model. Analysis of the residual trends and their variability under the alternative models then provides information on the limitations of the alternative parameter sets.

Data and Resources

We compiled the response spectra of ground motions for CENA earthquakes from the NGA-East flatfile provided by Christine A. Goulet (written commun., 2014). Ground-motion simulations were performed using the SMSIM v3.8 software that is available at http://www.daveboore.com/software_online.html (last accessed in October 2014). All graphics were produced using CoPlot software (www.cohort.com, last accessed in October 2014).

Acknowledgements

This study was supported by the Natural Sciences and Engineering Research Council of Canada, by the NGA-East project, and by the USGS NEHRP program under Grant G13AP00067.

References

Allen, T., P. Cummins, T. Dhu, and J. Schneider (2007). Attenuation of ground-motion spectral amplitudes in southeastern Australia, *Bull. Seism. Soc. Am.* **97**, 1279–1292.

Ancheta, T., R. Darragh, J. Stewart, E. Seyhan, W. Silva, B. Chiou, K. Wooddell, R. Graves, A. Kottke, D. Boore, T. Kishida, and J. Donahue (2014). PEER NGAWest2 database, *Earthquake Spectra*, **30**, 989-1006.

Atkinson, G. M. (2004). Empirical attenuation of ground-motion spectral amplitudes in southeastern Canada and the northeastern United States, *Bull. Seism. Soc. Am.* **94**, 1079–1095.

Atkinson, G. M. (2008). Ground motion prediction equations for eastern North America from a referenced empirical approach: Implications for epistemic uncertainty, *Bull. Seism. Soc. Am.* **98**, 1304–1318.

Atkinson, G. M. (2010). Ground-motion prediction equations for Hawaii from a referenced empirical approach, *Bull. Seism. Soc. Am.* **101**, 1304–1318.

Atkinson, G. M. (2012). Evaluation of attenuation models for the northeastern United States/southeastern Canada, *Seism. Res. Lett.* **83**, 166–178.

Atkinson, G. M., and D. M. Boore (1995). Ground-motion relations for eastern North America, *Bull. Seism. Soc. Am.* **85**, 17–30.

Atkinson, G. M., and D. M. Boore (2006). Earthquake ground-motion prediction equations for eastern North America, *Bull. Seism. Soc. Am.* **96**, 2181–2205.

Atkinson, G. M., and D. M. Boore (2011). Modification to existing ground-motion prediction equations in light of new data, *Bull. Seism. Soc. Am.* **101**, 1121–1135.

Atkinson, G. M., and D. Motazedian (2013). Ground-motion amplitudes for earthquakes in Puerto Rico, *Bull. Seism. Soc. Am.* 103, 1846–1859.

Atkinson, G. M., and W. Silva (2000). Stochastic modeling of California ground motions, *Bull. Seism. Soc. Am.* **90**, 255–274.

Babaie Mahani, A.., and G. M. Atkinson (2012). Evaluation of functional forms for the attenuation of small-to-moderate-earthquake response spectral amplitudes in North America, *Bull. Seism. Soc. Am.* **102**, 2714–2726.

Boore, D. M. (2003). Simulation of ground motion using the stochastic method, *Pure and Applied Geophysics*, **160**, 635-376.

Boore, D. M. (2005). SMSIM---Fortran programs for simulating ground motions from earthquakes: Version 2.3---A revision of OFR 96-80-A, U.S. Geological Survey Open-File Report, *U. S. Geological Survey Open-File Report* 00-509.

Boore, D.M. (2010). Orientation-independent, non geometric-mean measures of seismic intensity from two horizontal components of motion, *Bull. Seism. Soc. Am.* **100**, 1830–1835.

Boore, D. M. and E. M. Thompson (2014). Path durations for use in the stochastic-method simulation of ground motions, *Bull. Seism. Soc. Am.* **104**, 2541–2552.

Boore, D. M. and E. M. Thompson (2015). Revisions to some parameters used in stochastic-method simulations of ground motion, *Bull. Seism. Soc. Am.* **105**, (in review).

Boore, D. M., C. Di Alessandro, and N. A. Abrahamson (2014a). A generalization of the double-corner-frequency source spectral model and its use in the SCEC BBP Validation Exercise, *Bull. Seism. Soc. Am.* **104**, 2387–2398.

Boore, D. M., J. P. Stewart, E. Seyhan, and G. M. Atkinson (2014b). NGA-West2 equations for predicting response spectral accelerations for shallow crustal earthquakes, *Earthquake Spectra*, **30**, 1057-1085.

Brune, J. N. (1970). Tectonic stress and the spectra of seismic shear waves from earthquakes, *J. Geophys. Res.* **75**, 4997–5009.

Burger, R. W., P. G. Somerville, J. S. Barker, R. B. Herrmann, and D. V. Helmberger (1987). The effect of crustal structure on strong ground motion attenuation relations in eastern North America, *Bull. Seism. Soc. Am.* **77**, 420–439.

Campbell, K. W. (2002). Development of semi-empirical attenuation relationships for the CEUS, Report to U.S. Geological Survey, NEHRP Award No.01HQGR0011.

Campbell, K. W. (2003). Prediction of strong ground motion using the hybrid empirical method and its use in the development of ground-motion (attenuation) relations in eastern North America, *Bull. Seism. Soc. Am.* **93**, 1012–1033.

Chapman, M. C., and R. W. Godbee (2012). Modeling geometrical spreading and the relative amplitudes of vertical and horizontal high-frequency ground motions in eastern North America, *Bull. Seism. Soc. Am.* **102**, 1957–1975.

Chapman, M. C. (2013). On the rupture process of the 23 August 2011 Virginia earthquake, *Bull. Seism. Soc. Am.* **103**, 613–628.

EPRI (2004). CEUS ground motion project final report. Technical Report 1009684. Electric Power Research Institute, Dominion Energy, Glen Allen, VA, Entergy Nuclear, Jackson, MS, and Exelon Generation Company, Kennett Square, PA. Palo Alto, Calif.

Frankel, A. (2009). A constant stress-drop model for producing broadband synthetic seismograms: Comparison with the Next Generation Attenuation Relations. Bull. Seism. Soc. Am., **99**, 664-681.Hassani, B., and G. M. Atkinson (2014). Referenced empirical ground-motion model for eastern North America, *Seism. Res. Letters* (in review).

NEHRP (2000). *NEHRP Recommended provisions for seismic regulations for new buildings and other structures, Part 1, Provisions, FEMA 368*, Federal Emergency Management Agency, Washington, D.C.

Ojo, S., and R. Mereu (1986). The effect of random velocity functions on the travel times and amplitudes of seismic waves, *Geophysical Journal of the Royal Astronomical Society* **84**, 607–618.

Ou, G.-B., and R. B. Herrmann (1990). A statistical model for ground motion produced by earthquakes at local and regional distances, *Bull. Seism. Soc. Am.* **80**, 1397–1417.

Pezeshk, S., A. Zandieh, and B. Tavakoli (2011). Hybrid empirical ground-motion prediction equations for eastern North America using NGA models and updated seismological parameters, *Bull. Seism. Soc. Am.* **101**, 1859–1870.

Scherbaum, F., J. J. Bommer, H. Bungum, F. Cotton, and N. A. Abrahamson (2005). Composite ground motion models and logic trees: Methodology, sensitivities, and uncertainties, *Bull. Seism. Soc. Am.* **95**, 1575–1593.

Silva, W., N. Gregor, R. Darragh (2002). Development of regional hard rock attenuation relations for central and eastern North America, Report to Pacific Engineering and Analysis.

Somerville, P., J. McLaren, C. Saikia, and D. Helmberger (1990). The 25 November 1988 Saguenay, Quebec earthquake: Source parameters and the attenuation of strong ground motion, *Bull. Seism. Soc. Am.* **80**, 1118–1143.

Somerville, P., N. Collins, N. Abrahamson, R. Graves, and C. Saikia (2001). Ground motion attenuation relations for the central and eastern United States, Report to U.S. Geological Survey, NEHRP Award No. 99HQGR0098.

Somerville, P., R. Graves, N. Collins, S. G. Song, S. Ni, P. Cummins (2009). Source and ground motion models of Australian earthquakes, *Proceedings of the 2009 Annual Conference of the Australian Earthquake Engineering Society*.

Toro, G., N. Abrahamson, and J. Schneider (1997). Model of strong ground motion in eastern and central North America: best estimates and uncertainties, *Seism. Res. Lett.* **68**, 41–57.

Yenier, E., and G. M. Atkinson (2014a). Equivalent point-source modeling of moderate- to-large magnitude earthquakes and associated ground-motion saturation effects, *Bull. Seism. Soc. Am.* **104**, 1458–1478.

Yenier, E., and G. M. Atkinson (2014b). An equivalent point-source model for stochastic simulation of earthquake ground motions in California, *Bull. Seism. Soc. Am.* (in review).

Yenier, E., and G. M. Atkinson (manuscript in preparation). Modeling source and attenuation attributes of the 2010-2012 Christchurch, New Zealand earthquakes based on equivalent point-source modeling technique.

4 – Applications of Methodology to Rapid Determination of Moment and Stress, and to ShakeMap ground motions

The generic simulation-based GMPE developed in Section 3 has a variety of applications. Section 3 highlighted the use of the methodology to determine attenuation and source parameters. It was determined that events in CENA can be described by a bilinear attenuation form, with a geometric spreading of $R^{-1.3}$ to 50 km, followed by $R^{-0.5}$ at greater distances, with a frequency-dependent anelastic attenuation constant (γ as given in Table 3 of Section 3). The best average stress parameter, to match the spectral shape of events, increases with magnitude to a constant value near 300 bars for events of **M**>4. It also increases with focal depth, as shown in the figures in Section 3. Table 1 shows the individual source parameters for each of the events in the NGA-East database. In this table, the moment magnitudes are as assigned in the NGA-East database, while the stress parameter is the value that provides the best match to the spectral shape of the source spectrum (as obtained by playing back regional attenuation effects), for the specified moment.

Table 1 - Source Parameters of events in the NGA-East Database (PIE=1 for potentially-induced). Note that stress is based on spectral shape, and a calibration constant is needed to match the observed ground-motion levels (as discussed in Section 3).

EQID	nRecs	Earthquake Name	Year	Month	Day	Hour	Mw(NGA-e)	HypoLat (deg)	HypoLong (deg)	HypoDepth (km	PIE	BestStress (bar)
5	24	Saguenay QC	1988	11	25	23	5.8	48.10	-71.21	21.5	0	447
6	8	La Malbaie QC	1997	8	20	9	3.3	47.54	-70.29	7.5	0	56
7	9	La Malbaie QC	1997	10	28	11	4.3	47.67	-69.91	5.0	0	447
8	14	Cap-Rouge QC	1997	11	6	2	4.5	46.80	-71.42	22.0	0	891
9	9	Cote-Nord QC	1999	3	16	12	4.4	49.62	-66.34	20.0	0	708
10	5	Kipawa QC	2000	1	1	11	4.6	46.84	-78.93	13.0	0	398
11	10	La Malbaie QC	2000	6	15	9	3.3	47.67	-69.80	11.4	0	562
12	10	Laurentide QC	2000	7	12	15	3.7	47.55	-71.08	18.0	0	1000
13	6	Laurentide QC	2000	7	12	15	3.1	47.56	-71.06	18.0	0	794
14	12	Ashtabula OH	2001	1	26	3	3.9	41.87	-80.80	3.8	1	25
15	15	Enola AR	2001	5	4	6	4.4	35.21	-92.19	10.0	0	45
16	45	Au Sable Forks NY	2002	4	20	10	5.0	44.51	-73.70	11.0	0	316
18	16	Caborn IN	2002	6	18	17	4.6	37.98	-87.80	17.0	0	112
20	18	Charleston SC	2002	11	11	23	4.0	32.40	-79.94	9.0	0	1000
21	20	Ft Payne AL	2003	4	29	8	4.6	34.49	-85.63	12.0	0	447
22	11	Blytheville AR	2003	4	30	4	3.6	35.94	-89.92	23.0	0	18
23	10	Bardwell KY	2003	6	6	12	4.1	36.87	-88.98	2.0	0	10
24	25	La Malbaie QC	2003	6	13	11	3.6	47.70	-70.09	11.1	0	178
25	43	Bark Lake QC	2003	10	12	8	3.8	47.01	-76.36	18.0	0	794
26	19	Jefferson VA	2003	12	9	20	4.3	37.77	-78.10	10.0	0	1000
29	27	Prairie Center IL	2004	6	28	6	4.2	41.44	-88.94	7.0	0	316
30	35	Port Hope ON	2004	8	4	23	3.1	43.67	-78.23	4.0	0	89
31	17	Milligan Ridge AR	2005	2	10	14	4.1	35.75	-90.23	15.0	0	50
32	41	RiviereDuLoup QC	2005	3	6	6	4.6	47.75	-69.72	12.3	0	794
33	46	Shady Grove AR	2005	5	1	12	4.3	35.83	-90.15	8.0	0	56
34	40	Miston TN	2005	6	2	11	4.0	36.14	-89.46	15.0	0	100
35	66	Thurso ON	2006	2	25	1	3.8	45.65	-75.23	16.0	0	562
37	35	BaieSaintPaul QC	2006	4	7	8	3.8	47.37	-70.48	25.0	0	708
38	31	Ridgely TN	2006	9	7	13	3.4	36.27	-89.50	7.0	0	56
40	35	Acadia ME	2006	10	3	0	3.9	44.35	-68.15	2.0	0	20
41	19	Marston MO	2006	10	18	20	3.4	36.54	-89.64	8.2	0	10
46	58	Mt Carmel IL	2008	4	18	9	5.3	38.45	-87.89	14.0	0	282
47	55	Mt Carmel IL aftshk	2008	4	18	15	4.6	38.48	-87.89	14.0	0	178
48	52	Mt Carmel IL aftshk	2008	4	21	5	4.0	38.47	-87.82	15.0	0	141
49	47	Mt Carmel IL aftshk	2008	4	25	17	3.8	38.45	-87.87	13.0	0	100
50	25	Buckingham QC	2008	6	11	4	3.0	45.63	-75.38	18.0	0	282
51	30	RiviereDuLoup QC AS	2008	11	15	10	3.6	47.74	-69.74	13.3	0	224
56	119	Jones OK	2010	1	15	15	3.8	35.59	-97.26	8.0	1	16
57	114	Lincoln OK	2010	2	27	22	4.2	35.55	-96.75	4.0	1	45
58	57	Whiting MO	2010	3	2	19	3.4	36.79	-89.36	5.0	0	28
60	86	Val-des-Bois QC	2010	6	23	17	5.1	45.90	-75.50	22.0	0	447
61	31	St. Flavien QC	2010	7	23	17	3.5	46.58	-71.67	13.0	0	251
63	9	Mont Laurier QC	1990	10	19	7	4.5	46.47	-75.59	11.0	0	251
64	39	Montgomery MD	2010	7	16	4	3.4	39.17	-77.25	18.0	0	200
66	159	Slaughterville OK	2010	10	13	14	4.4	35.20	-97.31	14.0	1	141
67	79	Guy AR	2010	10	15	10	3.9	35.28	-92.32	5.0	0	28
68	42	Concord NH	2010	9	26	3	3.1	43.29	-71.66	3.4	0	20
73	126	Arcadia OK	2010	11	24	22	4.0	35.63	-97.25	3.0	1	28
74	119	Bethel Acres OK	2010	12	12	1	3.2	35.39	-97.00	4.0	1	10
75	46	Greentown IN	2010	12	30	12	3.9	40.43	-85.89	14.0	0	178
76	110	Guy AR	2010	11	20	19	3.9	35.32	-92.32	5.0	0	89
80	149	Greenbrier AR	2011	2	28	5	4.7	35.27	-92.34	4.0	1	63
81	169	Sullivan MO	2011	6	7	8	3.9	38.12	-90.93	27.0	0	141
82	36	Eagle Lake ME	2006	7	14	9	3.5	46.92	-68.68	17.0	0	50
85	68	Hawkesbury ON	2011	3	16	17	3.6	45.58	-74.55	7.0	0	355
86	8	CharlevoixSZ QC	2001	5	22	0	3.6	47.65	-69.92	11.4	0	1000
87	18	BaieSaintPaul QC	2002	8	17	5	3.2	47.33	-70.51	13.3	0	891
88	69	Mineral VA	2011	8	23	17	5.7	37.93	-77.98	5.8	0	178
89	60	Mineral VA aftshk	2011	8	25	5	4.0	37.94	-77.90	2.0	0	63
90	102	Sparks OK	2011	11	5	7	4.7	35.57	-96.70	3.0	1	35
91	88	Sparks OK	2011	11	6	3	5.7	35.54	-96.75	8.0	1	224
116	6	Saguenay FS	1988	11	23	9	4.2	48.13	-71.20	28.0	0	224
117	6	Saguenay AS	1988	11	26	3	3.5	48.14	-71.30	30.0	0	112

We can readily use the magnitude formula of Section 2 to determine the moment for any event that occurs, based on the response spectrum at 1Hz. Then we can use the GMPE of Section 3 to determine the implied value of stress from PSA at 10 Hz (a function of moment and stress parameter) - which is the value needed to correctly reproduce the observed amplitudes at higher frequencies. The procedure is as follows, with an example being given for the 2005 Riviere de Loup, Quebec earthquake in Table 2. Note that the vertical component is preferred, as described in Section 2, as it allows the initial approximation of negligible site response (i.e. we can assume $F_S = 0$). If only the horizontal component is available, an estimate of the value of the site response term F_S should be made using an appropriate generic site response model (e.g. as in Atkinson and Boore, 2006, or Boore et al., 2014, for example; see Section 3). It is recommended to consider only those records within 300 km to minimize the impact of attenuation on the estimated source parameters.

1. Using the values of PSA at 1Hz, apply Equation 2 from Section 2 to determine the value of **M** for each station. The event **M** is the average of these estimates.
2. Evaluate the magnitude effect term for the event magnitude, $F_{M,}$ for PSA at 10 Hz, using Equation 3 in Section 3.
3. For each recorded value of 10-Hz PSA (using ln Y, in g), subtract the attenuation and calibration constant effects, in order to isolate the source term effect. Specifically, from Equation 1 in Section 3, we can write: $F_E = \ln \mathrm{Y} - (F_Z + F_\gamma + F_S + C)$. Thus we evaluate F_E (for 10 Hz) at each station that recorded the event. We take the average over all stations to get the 10-Hz event value of F_E. [Notes: *(a)* if using the vertical component, we assume $F_S = 0$; (b) If the 10-Hz PSA is not available, the PGA could be used instead in this procedure, in which case we would evaluate the $F_{M,}$ $F_Z, F_\gamma, F_S,$ and C terms for PGA instead of 10 Hz; I prefer 10-Hz PSA as it is less sensitive to kappa effects.]
4. From Equation 2 in Section 3, we calculate the stress-effect term for the event (in ln units): $F_{\Delta\sigma} = F_E - F_M$, where F_M and F_E have been evaluated for the average event **M**, in steps 2 and 3.
5. Finally, we use Equation 4 from Section 3 ($F_{\Delta\sigma} = e_{\Delta\sigma}\ln(\Delta\sigma/100)$) to compute the stress parameter, $\Delta\sigma$. Note that the coefficient $e_{\Delta\sigma}$ is given as a function of magnitude by Equation 17 in Section 3. To evaluate it, we need to know whether the stress parameter will be greater or less than the reference value of 100 bars. This depends on the sign of $F_{\Delta\sigma}$, which will be positive for stress >100 bars, and negative for stress <100 bars.
6. Note that the value of **M** and stress could be refined if desired by iterating this procedure an additional time. We could make an improved estimate of **M**, using the 1-Hz PSA to evaluate F_E at 1 Hz, following the procedure that was used in Steps 2 and 3 for 10 Hz. We could then obtain a revised value of $F_{M,}$ at 1 Hz, as F_E - $F_{\Delta\sigma}$ (for our determined value of stress). We would then find the value of **M** (trying values slightly larger or smaller than our initial estimate) that produces the correct value of F_M. The advantage of this alternative would be to make the magnitude and stress estimates completely compatible. However, this iteration should not be necessary in general, as long as the initial value of **M** is reasonably well determined.

Table 2 – Example Calculation of Moment and Stress, as obtained following Steps 1 to 5.

Example Calculation of Event Moment and Stress for 2005 Riviere de Loup Event												s5	-2.45
				heff	5			gamm	-0.00564			s6	1.57
				e0	2.78	b3	-0.377	C	-0.172			s7	-0.289
		obs. In cgs units		e1	0.712	b4	0.0247	delb3	0.0727			s8	0.023
				e2	-0.262					Fstress=FE-FM		s9	-0.00066
			avg.M		FM-10hz					FE=lnY-(C+Fg+FZ)		egt100	0.598
		(cgs units	4.57		1.95				C+	2.34	0.39	193	
Rhypo~Reff	logZ	1hzPSAv	M(AGY14	10HzPSAv			FZ-10hz		Fg-10hz	FE-10hz	Fstress10	STRESS	
14.5	-1.51	3.72	4.55	151.67			-3.76		-0.25	2.15	0.20		
19.9	-1.69	3.02	4.61	30.43			-4.25		-0.28	1.06	-0.89		
21.7	-1.74	1.45	4.42	28.48			-4.39		-0.29	1.15	-0.80		
28.8	-1.90	5.68	4.95	188.49			-4.83		-0.33	3.51	1.56		
30.7	-1.93	3.87	4.86	46.24			-4.93		-0.35	2.22	0.27		
35.9	-2.02	2.42	4.78	29.57			-5.17		-0.37	2.05	0.10		
38.8	-2.07	1.34	4.64	41.76			-5.30		-0.39	2.53	0.58		
40.0	-2.08	1.27	4.63	33.81			-5.34		-0.40	2.37	0.42		
41.7	-2.11	0.53	4.39	7.19			-5.41		-0.41	0.90	-1.05		
45.8	-2.16	0.22	4.16	12.59			-5.56		-0.43	1.63	-0.32		
51.6	-2.22	1.20	4.71	28.52			-5.72		-0.46	2.64	0.69		
62.1	-2.26	1.35	4.78	49.77			-5.86		-0.52	3.40	1.45		
67.7	-2.27	0.57	4.54	19.22			-5.93		-0.55	2.55	0.60		
68.8	-2.28	4.36	5.15	45.82			-5.94		-0.56	3.43	1.48		
108.7	-2.38	0.41	4.53	15.17			-6.29		-0.79	2.90	0.95		
115.0	-2.39	0.17	4.28	12.66			-6.33		-0.82	2.80	0.85		
116.2	-2.39	0.47	4.58	4.24			-6.34		-0.83	1.72	-0.23		
117.0	-2.39	0.33	4.48	13.75			-6.34		-0.83	2.91	0.96		
159.5	-2.46	0.45	4.64	6.10			-6.58		-1.07	2.57	0.62		
159.7	-2.46	0.49	4.66	6.14			-6.58		-1.07	2.58	0.63		
190.7	-2.50	0.32	4.57	6.68			-6.72		-1.25	2.98	1.03		
212.0	-2.52	0.11	4.29	1.91			-6.80		-1.37	1.93	-0.03		
233.5	-2.54	0.11	4.30	1.37			-6.87		-1.49	1.79	-0.16		
259.7	-2.57	0.23	4.56	2.48			-6.95		-1.64	2.61	0.66		
267.9	-2.57	0.08	4.27	1.53			-6.98		-1.68	2.19	0.24		

It should be noted that the estimation procedure described in the foregoing is based on using the amplitude of PSA at 10 Hz to infer the stress that is compatible with the GMPE for the given moment, rather than using the spectral shape (as was done to derive the GMPE). The rationale is to allow an estimation of source parameters directly from ShakeMap ground motion parameters and simple formulae. The procedure will lead to values that should reproduce the average observed spectral amplitudes correctly, but may not match the corner-frequency-based stress drop. The reason is that the average value for the calibration constant is assumed in the generic GMPE (rather than an event-specific value being computed), and thus the stress parameter must take up any difference between event-specific and average calibration terms. This is why the 10-Hz PSA estimate of stress for the 2005 Riviere de Loup event in the example calculation is 193 bars (Table 2), while the spectral-shape based estimate from Section 3 is 794 bars (Table 1). The model moment magnitude (4.6) and stress (193bars),

when used in the generic GMPE model of Section 3, are the values which will correctly reproduce the average observed amplitudes, as illustrated in Figure 1.

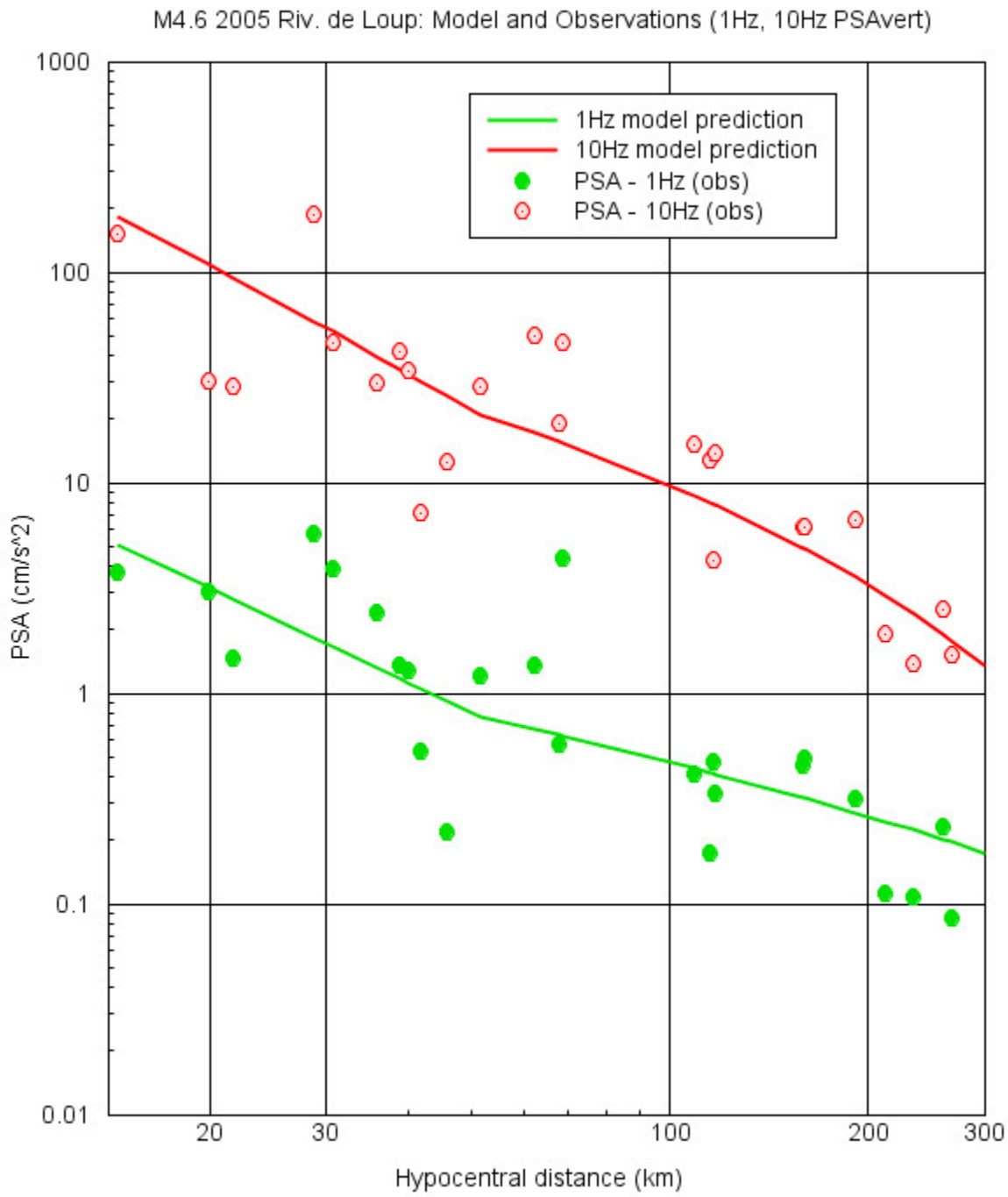

*Figure 1 – Comparison of PSA observations (vertical component) at 1Hz and 10Hz for **M**4.6 2005 Riviere de Loup event with model predictions for moment (**M**=4.57) and stress (193 bars) as derived using procedure in Steps 1 to 5.*

In conclusion, with the calibrated moment and stress values for the event determined, we can use the GMPE formulation in Section 3 to completely describe the ground motions for the event as a function of distance, for a reference ground condition. This event-specific GMPE, coupled with a regional grid of site amplification factors, F_S (such as those computed using Vs30 or other site amplification measures), provide the ground motions needed for producing reliable, calibrated ShakeMaps.

Acknowledgements:

This report makes use of collaborative work conducted with my Ph.D. students over the last several years, including in particular Alireza Babaie Mahani, Emrah Yenier and Behzad Hassani.